SIMBA

Système Intégré de Modélisation de la Baleine noire de l'Atlantique

(Integrated modelling system for the North Atlantic Right Whale)

WP3 – Species Distribution Modelling for the North Atlantic Right Whale

Lead: Frédéric Maps, Takuvik/U.Laval, Co-Lead: Arctus; Collaborators: Bigelow, NEA

Prepared by:

Andéol Bourguoin, Fanny Thiéry, Frédéric Maps

Version and Signature

Prepared by	Version	Date	Modifications
Andeol Bourguoin, Fanny Thierry	1.0	12/2023	Initial version
Verification by			**Modifications**
Fred Maps			
Final Authorization			**Signature**
Simon Bélanger			

EXECUTIVE SUMMARY

The North Atlantic right whale (NARW), classified as critically endangered, faces significant challenges to its existence, marked by historical population decimation due to commercial whaling. Despite protective measures since 1935, negative population growth rates have been observed since 2014, with ship strikes and fishing gear entanglements identified as major causes of death. Additionally, a shift in foraging areas since the mid-2010s, attributed to changes in prey distribution, has led NARWs into the Gulf of St. Lawrence, resulting in a surge in mortalities from increased maritime activities.

To address the challenges, the Canadian government regulates vessel traffic in areas prone to North Atlantic right whales. However, the vast geographic range and scarcity of the whales make effective mitigation challenging. The SIMBA project (Système Intégré de Modélisation de la Baleine noire de l'Atlantique) aims to enhance predictive capabilities regarding NARW distribution on the Northwest Atlantic shelf. Work Package 3 specifically focuses on understanding oceanographic and biological factors influencing NARW presence, with the goal of improving spatial predictions.

The present report provides an overview of the methodologies employed in this project designed to investigate the dynamics of North Atlantic Right Whales (NARW) in Canadian waters. The report emphasizes the significance of utilizing high-quality data, such as satellite-derived products and 3D models. Notably, the project explores innovative simulations of potential dense copepod aggregations, which represent the primary prey of NARWs. The study recognizes the critical interplay between predator and prey dynamics and highlights the decline of traditional foraging habitats, as well as the increased utilization of the Gulf of St. Lawrence due to prey scarcity.

Two distinct modelling frameworks were developed, each with a specific focus: one on Calanus dense aggregation areas, and the other on NARW distribution. Although integration efforts were not fully realized at the time of this report, both models are prepared for future integration. The results and predictions generated from these models represent a significant step towards achieving a comprehensive understanding of NARW dynamics in Canadian waters. The report concludes with a discussion of the implications of the findings and outlines future developments to further refine and integrate the modelling frameworks. The overarching objective remains to enhance predictive capabilities concerning the distribution of the vulnerable NARW population in the challenging and heavily trafficked waters of the Atlantic seaboard of the United States and Canada.

TABLE OF CONTENTS

Acronyms

BBP Particulate Backscattering Coefficient

BRT Boosted Regression Tree

CDM Colored Detrital Matter

CTA Classification Tree Analysis

DFO Department Of Fisheries And Oceans

ESA European Space Agency

GAM Generalised Additive Model

GBM Gradient Boosting Machines

Gom Gulf Of Maine

GSL Gulf Of St. Lawrence

LOPC Laser Optical Plankton Counter

NARW North Atlantic Right Whale

NASA National Aeronautics and Space Administration

NOAA National Oceanic and Atmospheric Administration

NRT Near Real Time

PAR Photosynthetically Available Radiation

PP Primary Production

RF Random Forest

ROC Receiver Operating Characteristic

SIMBA Système Intégré De Modélisation De La Baleine Noire De l'Atlantique (*Integrated Modelling System For The North Atlantic Right Whale*)

SDM Species Distribution Model

TSS Training Stress Score

List of Figure

1. Introduction

North Atlantic right whales (*Eubalaena glacialis* Müller 1776, hereafter called NARW) are currently classified as a critically endangered species (IUCN, 2020). In 2018, the only remaining population was estimated at 412 individuals (95%CI: 403–424; NOAA fisheries, 2021). Its population has historically been decimated by commercial whaling (Reeves et al., 2009). It is interesting to note that its very name, the right whale, may come from the fact that these were slow, feeding at the surface, and even floated once killed, hence being the "*right whales*" to hunt. Despite its protected status since 1935, and the end of whaling on this species, the population still struggles to recover. After a weak positive population growth rate during the 2000's and early 2010's, negative yearly gross rates have been steadily observed since 2014 (Pace et al., 2021, 2017). In recent decades, most of the identified causes of death are attributed to ship strikes and fishing gear entanglements (Knowlton et al., 2022). Even though identified death represent probably less than half of the death that occur (Pace et al., 2021), these mortality factors remain considerable (Knowlton et al., 2012, 2022; Laist et al., 2014; Meyer-Gutbrod and Greene, 2018; Moore et al., 2021; Vanderlaan et al., 2008).

Survival is not only about escaping injuries; for animals that large, it is essentially about finding food in sufficient quantity and of sufficient quality. Hence, prey availability and feeding grounds location was also identified as key factors controlling population viability. NARW migrate every year from calving areas in South-eastern U.S.A around winter to foraging areas in North-eastern America around summer (Gowan et al., 2019; Kenney et al., 2020), where these baleen whales feed primarily on dense aggregations of their preferred prey, the late copepodite stages of large *Calanus* species (Baumgartner and Mate, 2003; Beardsley et al., 1996; Mayo and Marx, 1990). During the foraging season, the capacity to store food supplies is essential for its fitness, i.e. its capacity to survive and produce viable offspring, as shown by the strong correlation between prey availability and their reproductive success (Hlista et al., 2009; Meyer-Gutbrod et al., 2015; Meyer-Gutbrod and Greene, 2018).

Individuals of the *Calanus* species are especially rich in lipids, a precious commodity for a marine mammal who's feeding apparatus has evolved to feed on them.

NARW usually find dense swarms of these tiny organisms either in surface waters where local circulation features tend to aggregate them, or close to the bottom of the continental shelf where currents, bathymetry and individual copepod's behaviour interact to somehow *trap* them in dense layers (Baumgartner and Mate, 2003; Beardsley et al., 1996; Mayo & Marx, 1990). Since they essentially rely on dense patches of *Calanus* spp. to satisfy their energetical needs, NARW have historically foraged in areas where such aggregations were commonly found, such as the Cape Cod Bay and the Great South Channel east of Massachusetts USA, and the Bay of Fundy and Roseway Basin in Canada (Davies et al., 2019).

However, a rather abrupt shift in the actual foraging area used by the NARW has been observed since the mid-2010s. The NARW's prey population is decreasing in their traditional feeding ground in the Gulf of Maine, Bay of Fundy and southern Scotian Shelf, while water temperature was rising in this area and circulation patterns were changing (Seidov et al., 2021; Grieve et al., 2017; Saba et al., 2016). The main hypothesis to explain this shift is a dramatic change in the distribution and abundance of *Calanus finmarchicus* that eventually led the NARW to look for new feeding grounds, especially further north of their usual areas, deep into the Gulf of St-Lawrence (Gavrilchuk et al., 2021; Meyer-Gutbrod et al., 2021; Meyer-Gutbrod and Greene, 2018; Pershing and Pendleton, 2021; Pershing & Stamieszkin 2020; Record et al., 2019). The high level of marine fishing and transportation activity in this area, combined with the novelty of this issue in Canada, have resulted in a spike in injuries and subsequent mortality by ship strikes and fishing gear entanglements. 2017 was a particularly critical year, when at least 17 whales died, so much so that these even made the news (ex. Press, 2017; NOAA fisheries, 2021).

The alarmingly small population of NARW continues to face profound challenges to its existence, largely due to the threats described previously and the simple fact that they live in one of the most heavily used coastal habitats in the world, the Atlantic seaboard of the United States and Canada. To minimize these mortality events, the Canadian government regulates vessel traffic in areas where NARW are likely to be present. This planification requires knowledge of the distribution of NARW. Surveys by boat and plane, acoustic sensors and calls for witnesses are used, but the area to cover is very large. Hence, it is not sufficient yet to prevent mortality events. To support these efforts, the SIMBA project (Système Intégré de Modélisation de la Baleine noire de

l'Atlantique) aims to predict right whales' changes in distribution over time on the Northwest Atlantic shelf.

As explained previously, right whales migrate north to build up their reserves during the productive season in these temperate, northern waters. Since they spend a significant part of their time foraging, their location is closely linked to that of their prey (Meyer-Gutbrod et al., 2015). Some models targeting right whale prey distribution already exist, but mostly at large temporal scales, typically seasonal, and aimed at explaining distributions of past years (ex. Brennan et al., 2021; Maps et al., 2011; Plourde et al., 2019; Sorochan et al., 2021; Zakardjian et al., 1999). A predictive model on a short time scale (i.e. predicting the near future of a few days) would provide useful knowledge to understand right whale movements. On the other hand, a coarser predictive model on a larger time scale (several months) could support the latter by making it possible to anticipate global right whale movements further in advance.

Understanding the habitat dynamics of species is a key part of making better predictions of their spatial distribution, as well as making more accurate recommendations for determining protected areas locations and establishing restrictions in space and time for human activities. **The aim of this Work Package 3 was to be able to make more accurate predictions of NARW presence in its new summer habitat** by identifying oceanographic and biological factors that explain most of the variability in NARW probability of presence at different space and time scales.

To achieve that goal, we have been working on two types of models, i.e. 1) 3D copepod aggregation modeling (Ph.D of A. Bourgouin) and 2) NARW habitat distribution modelling (Ph. D. of F. Thierry). Both models will be combined in the future as the first model will provide input to the second model (SDM).

The significant increase in data quality and quantity obtained in this project (i.e. satellite-derived products and 3D models output) are instrumental to make better predictions of NARW distribution at high spatial resolution. Moreover, one innovative avenue was to simulate areas of potential dense aggregations of large copepods, NARW's preferred prey. Copepods can voluntarily change depth by vertical migration (Genin et al., 2005; Maps et al., 2011; Woodson and McManus, 2007), leading over time to significatively different distributions from a particle passively transported by the currents (Genin et al., 2005; Maps et al., 2011; Sorochan et al., 2021; Zakardjian et al., 1999). Since the recent increase in frequentation of the Gulf of St. Lawrence seems driven

more by a decline in prey in traditional foraging habitats rather than by an increase in prey in this "new" feeding ground (Meyer-Gutbrod et al., 2022), better understanding the predator/prey dynamic between NARW and its preferred preys was a desirable aspect of our approach. The ultimate objective was to use these results as an additional dynamic layer of information to build models predicting the distribution of NARW itself. We did not manage to fully integrate both efforts (*Calanus* dense aggregation areas and NARW distribution models) by the time of this report, but we have created and tested both modelling framework that can be integrated in a near future.

We describe in the following sections both methodological approaches, their results and predictions, and discuss future developments to serve the overall objective of enhancing our predictive capabilities of the distribution of the scarce population of NARW in Canadian waters.

2. Geographical framework

The prediction of potential aggregation areas for the preferred preys of NARW will be focused on the coastal regions of the Northwest Atlantic (Figure 1): the estuary and Gulf of St. Lawrence (GSL), the Scotian Shelf, and the Gulf of Maine (GoM). This area is the preferred feeding habitat of NARW although, on rare occasions, some individuals are found at distant locations (e.g. in Iceland; see Hamilton, 2018). Furthermore, this area reports most of the events of collisions and entanglements in fishing gear, due to overlapping fishing activities and NARW feeding grounds. The ocean basin will not be included in the predictions, since it is not a foraging habitat of the NARW.

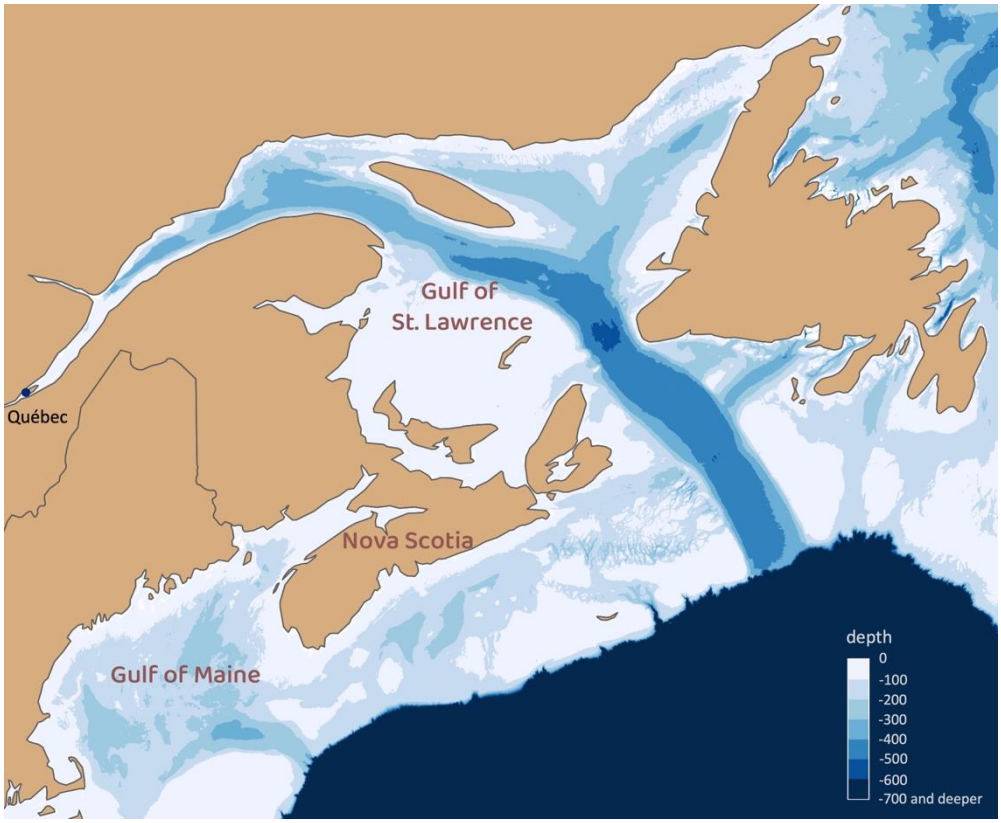

Figure 1. Geographical representation of the areas that will be targeted during the project. The bathymetry of the continental shelf is represented on a discrete scale with 100 m laps.

3. Prediction of potential foraging areas for the North Atlantic right whale in its main summer habitat

3.1. Methods

3.1.1. Target species

Two copepod species will be the focus of this thesis since they are of the preferred prey of right whales: *Calanus finmarchicus* and *C. hyperboreus (Figure 2)*. The right whales feed on zooplankton, and almost exclusively on calanoid copepod species. Its baleens form a sieve whose size can filter relatively small individual zooplankton (>333 micrometres, Mayo et al., 2020), and it has been observed historically to feed among large aggregations of *C. finmarchicus* occurring in areas recurrent enough to be identified as their usual feeding ground (Baumgartner et al., 2017, 2003; Baumgartner and Mate, 2003; Beardsley et al., 1996; Mayo and Marx, 1990). In addition, breeding success of right whales seems to increase during periods when *C. finmarchicus* abundance over the feeding grounds is higher than average (Hlista et al., 2009; Meyer-Gutbrod et al., 2015).

In the region that we study, *C. finmarchicus* and *C. hyperboreus* are the main contributors in the zooplankton community in terms of biomass (Runge and Simard, 1990; Sameoto and Herman, 1990; Kane, 2008; Lehoux et al., 2020; Gavrilchuk et al., 2020, 2021; Sorochan et al., 2021). The former is ubiquitous, while the latter is seasonally dominant in the GSL, where it has been increasingly present over the past ten years (Sorochan et al., 2019). The actual role of *C. hyperboreus* as a right whale prey is not clearly understood currently, but since it has a similar overall behaviour and morphology as *C. finmarchicus*, while packing about ten times more lipid than its boreal congener (Daase et al., 2021), it can be assumed that it is a potentially important prey for NARW. A third calanoid species, *C. glacialis*, is usually highly represented in subarctic systems, but it has never been abundant enough in the targeted area to be worth studying in this context.

Despite their numerous similarities, both *Calanus* species have different life history strategies, feeding strategies and distinct depth distribution resulting in potentially contrasting interactions with the currents in this dynamic system (Daase et al., 2021; Maps et al., 2014). Separate models were therefore created to study the

distribution of four distinct groups of prey: the two target species, each at an early and late stage of development.

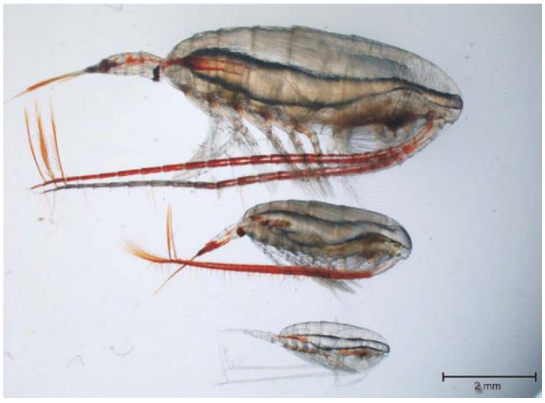

Figure 2. Pictures representing on the same scale, from up to down, Calanus hyperboreus, C. finmarchicus and C. glacialis. Picture: Malin Daase (Vogedes, 2014). The lipid content in the body of the individuals is clearly visible.

3.1.2. Modeling zooplankton aggregations

To predict aggregations of NARW preys, we simulate the trajectory of particles representing these preys, based on currents and their vertical position, and predict where these trajectories form dense aggregation areas (Figure 3).

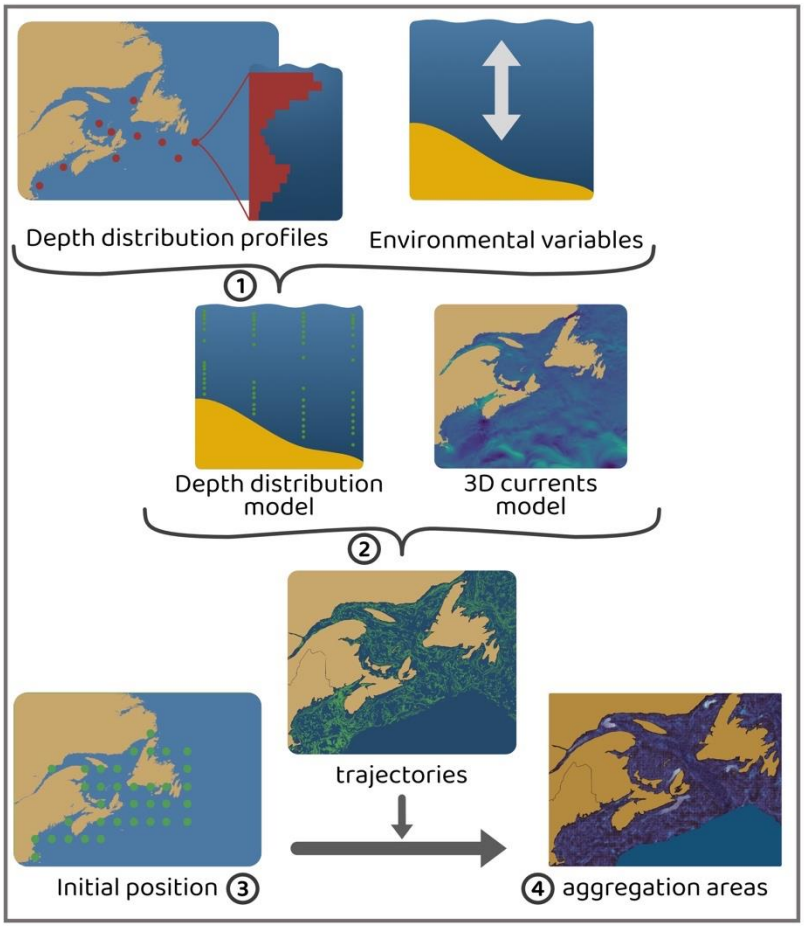

Figure 3. Scheme describing the method used to predict the potential areas of right whale prey aggregation. First (1), depth distribution models for Calanus finmarchicus and C. hyperboreus at distinct stages are built, based on the correlation between depth distribution profiles from the field, and bottom depth. Then (2), this depth distribution model is coupled with the CIOPS-E model that predicts currents in 3D, to determine the trajectories of the simulated NARW prey. For the simulation, an initial position of these particles is needed (3). And finally (4), based on the simulations, a map of the potential aggregation areas is created.

The first step was to build an agent-based model that predicts the depth distribution of the preferred prey species and development stages, as a function of several environmental parameters (Figure 3-1). To position particles in the water column, this model requires the preferred depth and spread of individuals around it for each target species and stages. These are estimated thanks to dataset of depth-stratified sampling (section 3.1.3).

The vertical position of the particles has a strong influence in their resulting distribution owing to the complex sheared circulation characteristic of this continental shelf system (Figure 3-2). The simulated particles are advected horizontally by the simulated currents, while moving vertically in relation to environmental variables according to the previously established model. As a result, the agent-based model has been coupled to outputs from a high-resolution regional circulation model, the *Coastal Ice-Ocean Prediction System for the East Coast of Canada* (CIOPS-E), which is derived from the Regional Ice-Ocean Prediction System (RIOPS) model run by ECCC for ocean and weather forecasts (Smith et al., 2021). It covers the north-western Atlantic Ocean with a highly accurate spatial resolution (1/36°, ~2-2.5 km in the GSL).

To simulate the spatiotemporal trajectories of prey-like particles, they must be assigned to an initial position. This position follows a regular gridded pattern covering the whole study area (Figure 3-3). The objective of this approach is to determine the location of all *potential* aggregation areas, regardless of the actual presence (or absence) of copepod supply. These simulated areas could highlight oceanographic features that the NARW seek out for foraging purposes, even though no actual feeding is taking place there.

Finally, once the trajectories have been simulated from an initial distribution pattern, a particle density is calculated over the entire study area to determine the aggregation areas (Figure 3-4). The calculation of this density is integrated after the particles have been allowed to circulate for a set amount of time.

3.1.3. Data

To predict the depth distribution of the NARW prey, we can count on a very comprehensive dataset provided by DFO that assembled depth-stratified net sampling of zooplankton where *C. finmarchicus* and *C. hyperboreus* individuals were identified at the development stage level (Figure 4). It covers 19 years of sustained sampling carried over all seasons, at several times of the day, and a large swath of our study area, including the Estuary and GSL, the Gulf of Maine, the Scotian Shelf and Newfoundland shelves. In parallel to the abundances of both target species, several environmental parameters were measured during the sampling. Some unavailable environmental data such as water mass stratification can be found separately from the dataset, using regional circulation models.

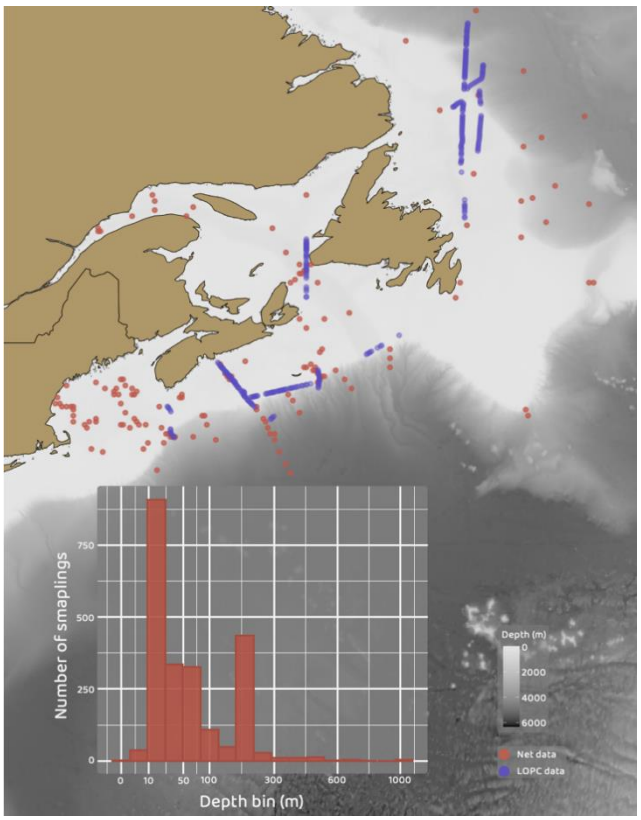

Figure 4. Map of station locations and histogram of the samplings' depth bins of the net dataset (square root transformation applied on the depth bin axis). Net dataset is represented in red, and laser optical plankton counter (LOPC) dataset in blue.

One major constraint, however, is that the width of the sampled depth strata in the dataset are different from one sample to another and can be quite large (Figure 8). This limits the potential quality of the depth distribution predictions. Another dataset will give access to a finer vertically resolved data (Figure 3). The latter gathers depth transects of adult *Calanus*-sized particle count, acquired by a laser optical plankton counter (LOPC).

Particles with a computed equivalent spherical diameter from 1000 µm to 2500 µm, and with attenuation proportion from 0 to 0.6 were selected as Calanus finmarchicus of stage CV, following the method of Pershing *et al*., (2012). In this publication, some LOPC profiles have been compared to concurrent ring net tows, and late *C. finmarchicus* dominates this size class in the nets. Furthermore, others have used the LOPC under this assumption (Checkley et al. 2008, Gaardsted et al. 2010). The detected particles are gathered in 10 meters bins to have density information, in a trade-off between high resolution and sufficient information in each bin. This information is collected from several horizontal transects on the GSL, the Scotian Shelf and Newfoundland shelves.

Based on these data, we regressed the *preferred depth* and *spread* parameters to environmental variables (section 3.1.4). Several variables have been tested, but eventually only the bottom depth has been kept, because it was the most significant, most consistent, and the easiest to use in the global mode. The *preferred depth* and *spread* parameters are obtained for each combination of *C. finmarchicus, C. hyperboreus* at young and late stages.

3.1.4. Depth distribution of zooplankton

This model simulates the temporal evolution of the vertical distribution of particles (i.e., calanus), representing the species at the different stages as a function of environmental conditions (Figure 5). As a result, it depends at each time step on the distribution of the particles at the previous time step. The algorithm used is an Ornstein-Uhlenbeck (O-U) process (Cheridito *et al.*, 2003), which simulates the evolution of a particle as a stochastic process around a target; it is also known as a "directed random flight". The discretized equation of the model is written as follows:

$$Z_t = \mu + (Z_{t-1} - \mu) \times e^{-\theta dt} + \sigma \times \sqrt{\frac{1 - e^{\theta dt}}{2\theta}} \times N_{0,1}$$

- Z_t is the current depth of the simulated particle at time *t.*
- μ is the preferred depth of the particle at time *t*. This parameter is determined in relation to the bottom depth (see below).
- σ, often named the volatility, parametrizes the impact of random fluctuations in the trajectory of a particle. These random fluctuations represent both the variability in

the swimming of a particle and the impacts of weak vertical turbulence. For a set of particles, it therefore parameterized the spread of the vertical distribution around μ. A different value of this parameter is determined for each of the species at young and late stages.

- *N (0,1)* is a random normal variable with mean 0 and variance 1.
- $\boldsymbol{\theta}$, the swimming speed or more accurately the vertical velocity, is set at 5 mm s^{-1}, as fixed for the same species and stages in a similar model by (Sorochan et al., 2021). The vertical velocity is assumed to include any effect of vertical currents, as these are most of the time at least one order of magnitude smaller than the copepod's swimming speed at the spatial resolution of the regional circulation model we use (Zakardjian et al., 1999; Zakardjian, 2003).
- *dt* represents the duration of the time step.

The values of the parameters μ and $\boldsymbol{\sigma}$ for each vertical profile sampled are determined by a cost minimization function (Price, 1977; Soetaert *et al.,* 2009) with a *mean absolute error* cost function. Correlative models are then used to establish the relationships between the determined μ and selected environmental variables (figure 5). Only the *bottom depth* variable has been correlated with μ. Since $\boldsymbol{\sigma}$ could not be correlated to any independent variable, its value is averaged for each species and stage. The models are weighted least squares regressions that integrate a variance increasing with the relationship, since as the bottom depth increases, the values of μ may differ. The uncertainty in the value of μ is large and correlated with bottom depth. This correlation is therefore calculated and added to the $\boldsymbol{\sigma}$ values as an uncertainty factor in the predictions.

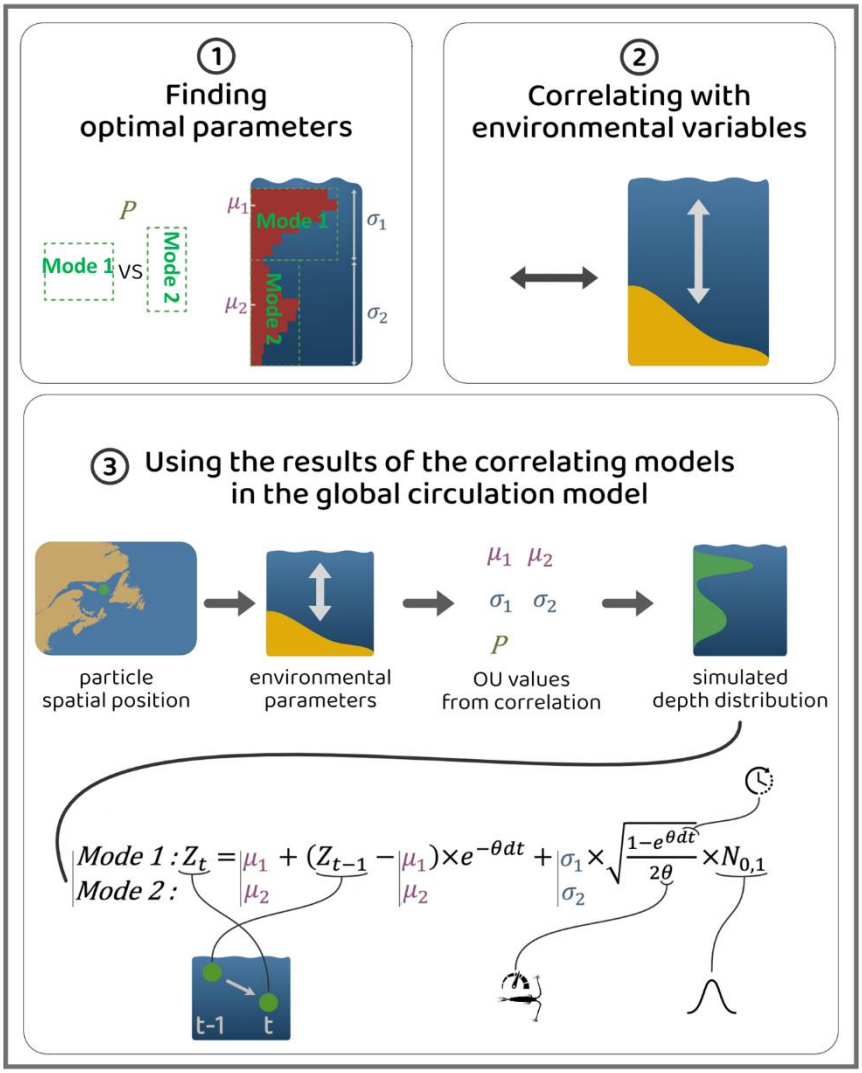

Figure 5. Scheme describing the depth distribution models for Calanus finmarchicus and C. hyperboreus at different stages based on the discretized equation of an Ornstein – Uhlenbeck (O-U) process.

An O-U process is unimodal and does not consider the possibility of several optimal depths. However, depth distribution data regularly show a bimodal curve (Figure 5). This could be represented by two O-U processes fitted simultaneously. The correlative models will then link the two couples of optimal parameters to environmental conditions: μ_1 of the upper mode, σ_1 of the upper mode, μ_2 of the lower mode, σ_2 of the lower mode, and a parameter p that records the importance of one mode versus the other among the population of particles. The value of μ_1 is limited from the shallowest depth sampled to half the bottom depth, and μ_2 from that value to the deepest depth sampled. Thus, when a distribution is unimodal (e.g. Figure 6-B), it is largely explained by either μ_1 or μ_2.

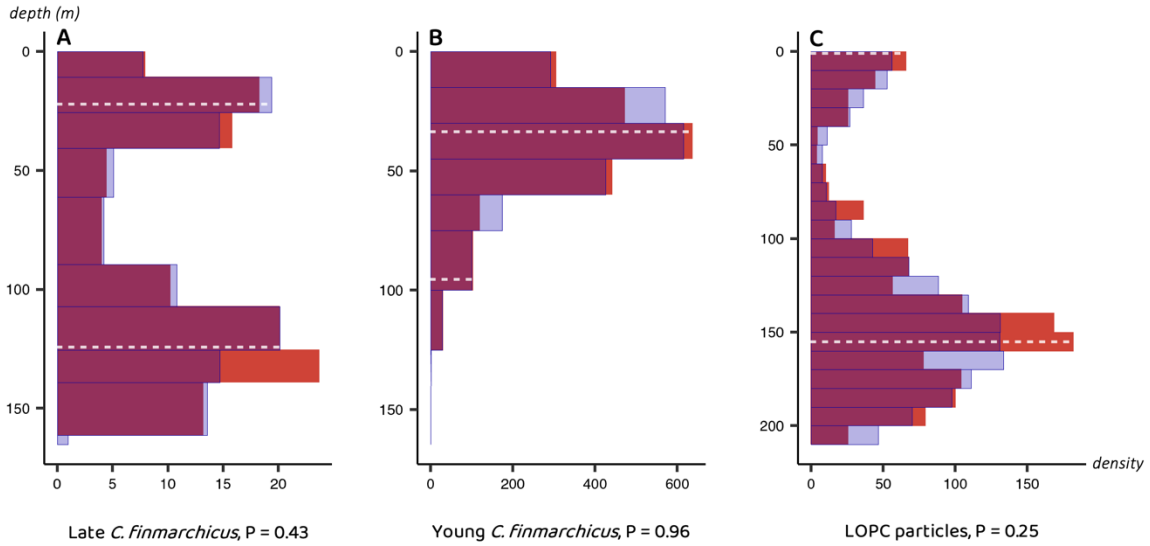

Figure 6. Examples of depth profiles observed (in orange) and simulated (in transparent blue). White dotted lines represent the values of μ. The profile A displays a typical bimodal distribution while the profile B displays a typical unimodal distribution close to the surface. The profile is derived from LOPC data.

The bottom depth of the study area follows a bimodal distribution, most of it being on the continental shelf with an average depth of approximately 150 m, the remainder being on the deeper abyssal plain, slightly above 5000 m (Figure 6-A). Since late development stages of *C. finmarchicus* and *C. hyperboreus* can both perform diel vertical migrations and overwinter at deeper depth than what the continental shelf allows (Heath *et al.*, 2004; Hirche, 1996c; Visser *et al.*, 2017), the bottom depth is therefore a potential constraint in a large part of the study area. Within the continental shelf, the topography also describes a bimodal distribution, with some areas such as the Laurentian Channel being deeper than several shallow plateaus (Figure 6-B). The constraint imposed by the bottom depth can therefore be of different importance, leading to a potential diversity of prey distribution patterns for NARW.

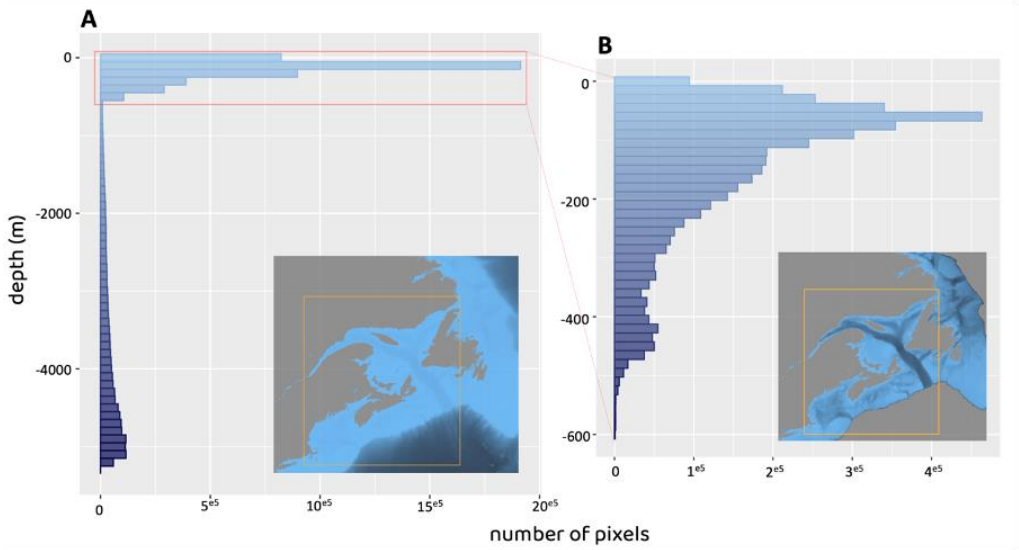

Figure 7. Frequency distribution of the bottom depth in the study area, geographically delimited by the orange square on the map, considering all the topography (A) and just the shelf (< -600 m) (B).

3.1.5. Predict the potential aggregation areas of right whale preferred preys

The methodology used to predict potential NARW prey aggregation areas is based on Maps *et al*. (2015) that predicted dense aggregation zones of krill in the GSL: these preys will be simulated as numerical particles evolving in the three-dimensional current output from the CIOPS-E model. At each timestep, the particle moves vertically based on environmental parameters and its depth at the previous timestep, according to the parameterised O-U process described above. Then particles are carried along by horizontal currents. Each day, we set new initial particles position, then run a simulation from several days backward in time and determine potential aggregation areas. This is done for the four combinations of prey species and development stages (young and late). We limited the simulations to the months of April to October, when most of the NARW sightings are reported in the GSL.

Output from the CIOPS-E model are available at two different timescales: daily averaged currents from 2017 to 2020, and hourly currents from 2021 onwards. The coupled model operates with a 30-minute time step, interpolating currents from these inputs. This time was chosen as a trade-off between precision and computational cost: it can capture tidal frequencies that have a major impact on surface circulation features, such as tidal and inertial currents, as well as the diel vertical migrations of the numerical particles whose interaction generates the dynamics of simulated prey aggregations.

The particles trajectories simulated by the hydrodynamic model can be analyzed from two different perspectives. On one hand, we can count the density of particles passing through grid cells in the study area at each timestep and observe how these densities change over time: this is the Eulerian approach. On the other hand, each particle's trajectory can be computed and the relative distances between all particles over time can allow us to determine areas where particles are converging (aggregating): this is the Lagrangian approach.

Currently, only the Eulerian approach has been implemented. We use 2 particles per grid cell to initialize the simulations, for a total of 756,904 particles uniformly distributed. Preliminary experiments showed that this number is sufficient to reveal clear patterns of particles aggregation. In the near future, another initialization pattern could be used based on improving knowledge of the copepod distribution in the study area. Efforts are currently made by Canadian and American research teams to correlate observations of copepod distributions integrated in the water column and environmental variables obtained from satellite imagery. These are promising analyses, capable of providing spatially extensive estimations used to initialize and validate our model outputs.

Particles trajectories are simulated for 8 days, and then the particles density is averaged from the particle's positions in the last 6 days. The first 2 days are not included because they act as burn-in to get rid of the imprint of the uniform initial disposition of the particles. The duration of the particles transport was chosen to highlight clearly the sub-mesoscale patterns of currents (Figure 11), and because the total time of 8 days is the timestep used as inputs for the simulation of the NARW habitat quality (section 4.1.1 below), for which these results will be used as inputs eventually.

Lagrangian analyses will soon be developed. Several Lagrangian metrics exist to determine the areas of numerical particles aggregation. We will use the finite-time Lyapunov exponents (FTLE). They compute aggregation areas in a cell by placing one particle at the center of each one, then moving them backwards in time within the model, until the target duration has been reached.

The density maps of the 4 groups of *Calanus*-like particles obtained from the models will be publicly available and regularly updated on a portal web maintained by the Hatfield teams (WP4). To run regularly, the model only needs inputs from the CIOPS-E model. Our ECCC partners will provide regular access to this data, and this frequency

will dictate how long it takes for the maps to be updated on the website. Ultimately, these maps will also be used as inputs for NARW's niche prediction models, the results of which will also be served on Hatfield's portal.

3.2. **Results**

3.2.1. Depth distribution models

The results of the depth distribution models are summarized in table 1 and in figure 8. For each species-stage combination, the upper panel (A) represents the ensemble of observations. It shows normalized concentrations as a function of depth, with the profiles grouped and averaged by bottom depths. The lower panel (B) shows the parameterized optimum values $\mu 1$ and $\mu 2$ as a function of the same bottom depth profile, along with the regression line fitted. Finally, the right-hand panel (C) is the resulting probability distribution as a function of for the simulated particles following either the upper or lower mode of distribution. The depth of these particles was simulated using an O-U process following the optimized parameters of the vertical distribution models, for a bottom depth of 300 m.

Table *1* The different values of the optimized parameters of the depth distribution models. bd = bottom depth.

	Late C. hyperboreus	*Young C. hyperboreus*	*Young C. finmarchicus*	*Late C. finmarchicus, LOPC data*	*Late C. finmarchicus, nets data*
Number of profiles	76	47	219	442	628
Mu1	0.3276101	0.2873384	0.1405234	0.2659345	0.2010376
Mu2	0.8276709	0.7446133	0.7199184	0.7924119	0.7346296
Sigma1	0.8187261 + 0.01541352 bd	0.5707538 + 0.01409882 bd	0.4714954 + 0.009404045 bd	0.7300764 + 0.01166824 bd	0.6400003 + 0.01314076 bd
Sigma2	0.8751834 + 0.009554192 bd	0.6450958 + 0.01423661 bd	0.6849555 + 0.009917493 bd	0.6765665 + 0.01005665 bd	0.8222354 + 0.01314954 bd
P	0.3071252	0.5218566	0.8307267	0.4862699	0.5950432

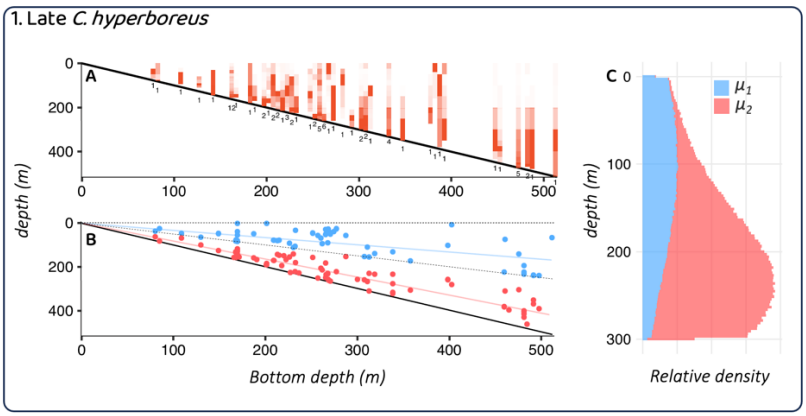
1. Late C. hyperboreus
A
B
C
depth (m)
Bottom depth (m)
Relative density
μ_1
μ_2

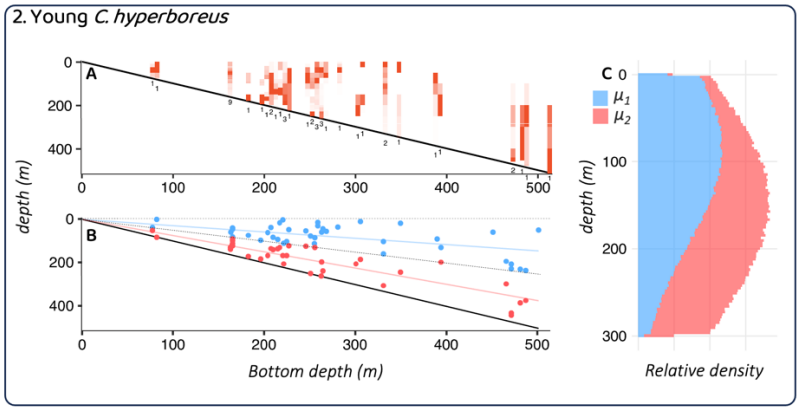
2. Young C. hyperboreus
A
B
C
depth (m)
Bottom depth (m)
Relative density
μ_1
μ_2

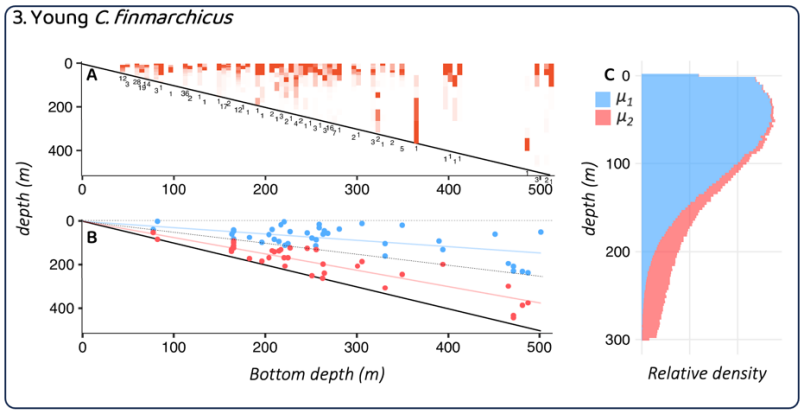
3. Young C. finmarchicus
A
B
C
depth (m)
Bottom depth (m)
Relative density
μ_1
μ_2

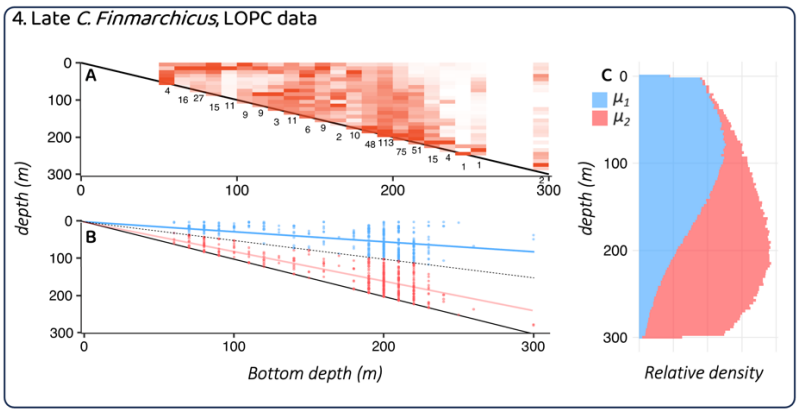
4. Late C. Finmarchicus, LOPC data
A
B
C
depth (m)
Bottom depth (m)
Relative density
μ_1
μ_2

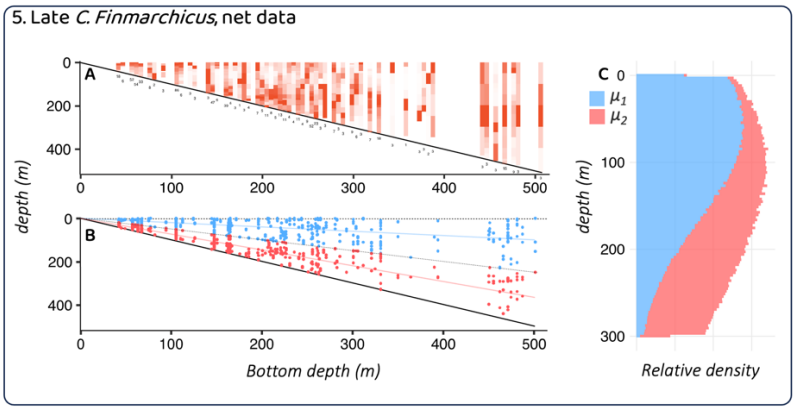

Figure 8. Results of the depth distribution models for 4 combinations of species and development stages and two different sources of data (Krumhansl et al. 2018 meta-analysis and LOPC samples). A) represents the depth distribution of individuals from the net profile. The transparency is an indicator of relative density, from 0 to 1. For each 10 meters bin of bottom depth, the number of profiles averaged is written. B) represents the upper and lower optimal depths (μ1 in blue and μ2 in red) obtained from the profiles. The two dotted lines represent the surface and the mid depth. The color lines represent the regression lines. C) is a representation of the depth distribution of 10,000 particles following an Ornstein-Uhlenbek equation with the values of the parameters obtained for late C. hyperboreus individuals.

The simulated distribution profiles show three different patterns of vertical distribution: *Late C. hyperboreus* particles that are close to the bottom, *Young C. finmarchicus* particles that are close to the surface, and *Late C. finmarchicus* (from vertical net data) and *Young C. hyperboreus* individuals that show no clear pattern related to the bottom depth. *Late C. hyperboreus* have long diapause periods, which could explain their distribution closer to the bottom. *Young C. finmarchicus*, on the other hand, are usually actively feeding in the productive surface layers. These three different patterns should result in three different dense aggregation patterns and could therefore have an impact on right whale food availability.

It appears important to note that the profiles of *Late C. finmarchicus* sampled by the LOPC and the resulting vertical distribution models is different than the one obtained from vertical net data: the former produce a clearer distinction between the surface and deeper modes ($\mu 1$ and $\mu 2$). It seems to reflect more effectively the expected distribution of diapausing late stages, and it may reflect the fact that net samples are dominated by sampling occurring earlier in the season, before diapause was widespread in the population. As a result, we will use the vertical profile parameterized from the LOPC dataset.

3.2.2. Potential aggregation areas of right whale preferred preys

We illustrate how the potential areas of dense aggregation appear with simulation results for each of the 4 species-stage group. Simulations are forced with hourly currents for the months of April and May 2022, and with daily averaged currents for the year 2018. An animation showing how these results evolve along 2018 is available in the appendix. The first element to consider when computing areas of dense aggregation is the advection duration (Figure 9). A time integration of 8 days presents the clearest areas of dense aggregation as it allows particles to travel sufficient distance to be trapped in sub-mesoscale advective features, while remaining cohesive. It shows the importance of choosing a sufficiently long aggregation time to observe patterns of aggregation areas that signal processes strong and recurrent enough to be noticeable at this scale.

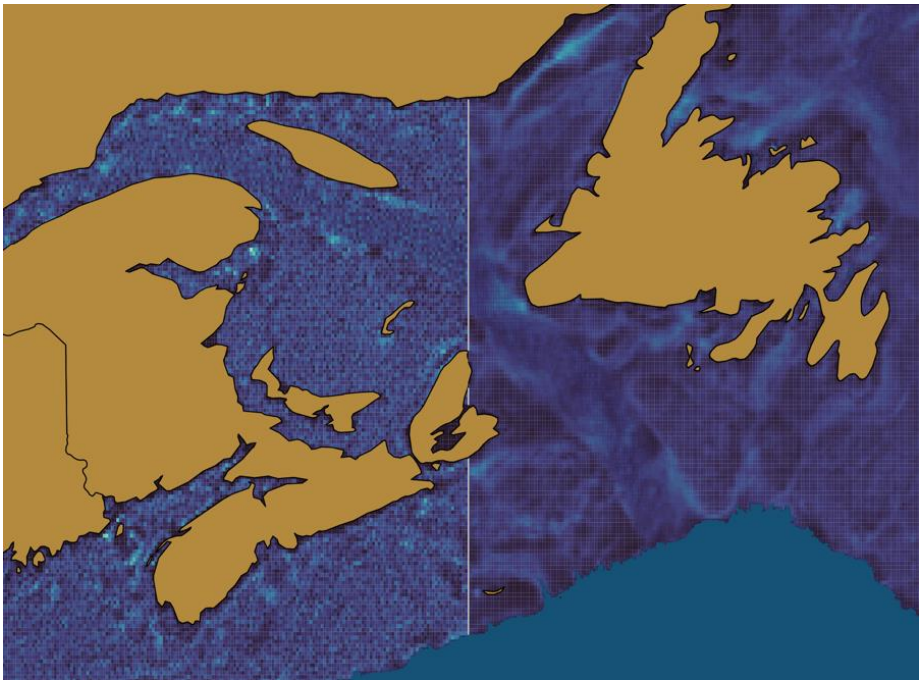

Figure 9. Example of a map obtained from densities vertically averaged after 2 hours of particles' advection on the left, and after 8 days on the right.

Maps of potential aggregation areas for young *C. finmarchicus* and late *C. hyperboreus* individuals in 2018 (Figure 10) reveal some similarities and contrasting patterns that can be explained by circulation features in the GSL (Figure 11). Outputs show rapid temporal variations from one 8-day period to the next (see the animations in the appendix, and Figure 10-2 and 10-3). This supports the hypothesis of a dominant role of advection by currents in spatio-temporal variations in the distribution of NARW prey.

For instance, the Gulf of Maine and the mouth area of the Bay of Fundy show significant and complex aggregation patterns. These are probably caused by the complex bathymetry and tidal currents in the area. In these areas, NARW sightings regularly correspond to predicted young *C. finmarchicus* aggregation zones (see Figure 10-A1 and 8-A2). It is interesting to point out that the head of the Laurentian channel (southeast of the Saguenay Fjord mouth) is also regularly predicted to be one of the strongest potential aggregation zones. This zone is known as a hot spot for numerous species of baleen whales that come there to feed during the whole feeding season, and NARW are no exception, even though they do not seem to be present in large numbers yet.

Outputs from young *C. finmarchicus* and late *C. hyperboreus* particles have many similarities, especially in shallow areas such as the Gulf of Maine and the Magdalen shallows. These areas somehow level the field for both types and constrain late *C. hyperboreus* particles to have a shallow distribution, similar to that of young *C. finmarchicus* particles. Indeed, the major differences seem linked to the bathymetry discontinuities. As an example, late *C. hyperboreus* particles form recurrent aggregations by the edges of the Laurentian Channel (Figure 10). The Madelaine Banks form the most recurrent area of NARW occurrence in the GSL. In summer 2018, the west of this area was busy with NARW, as can be seen from the sightings on all the maps in Figure 10. This does not match areas where the model predicts the strongest aggregations, but rather the most recurrent. It is interesting to note that the shallow depth there makes prey much more accessible to NARWs. If we focus solely on the Magdalen Islands banks, we can see that for the late *C. hyperboreus* predictions in particular, the whale occurrences are present in a relatively large aggregation area, at the edge of a very dark zone (void of aggregations). This zone appears to be the shallow extension of the Acadian Peninsula. The Gaspesian current slides along the southern edge of this peninsula, where the prey aggregates.

These observations indicate that the aggregation of prey determined by our models could explain part of the distribution of NARWs in their summer habitat. These results will be used as an additional information layer for the SDMs models computing habitat suitability scores for NARW (see below).

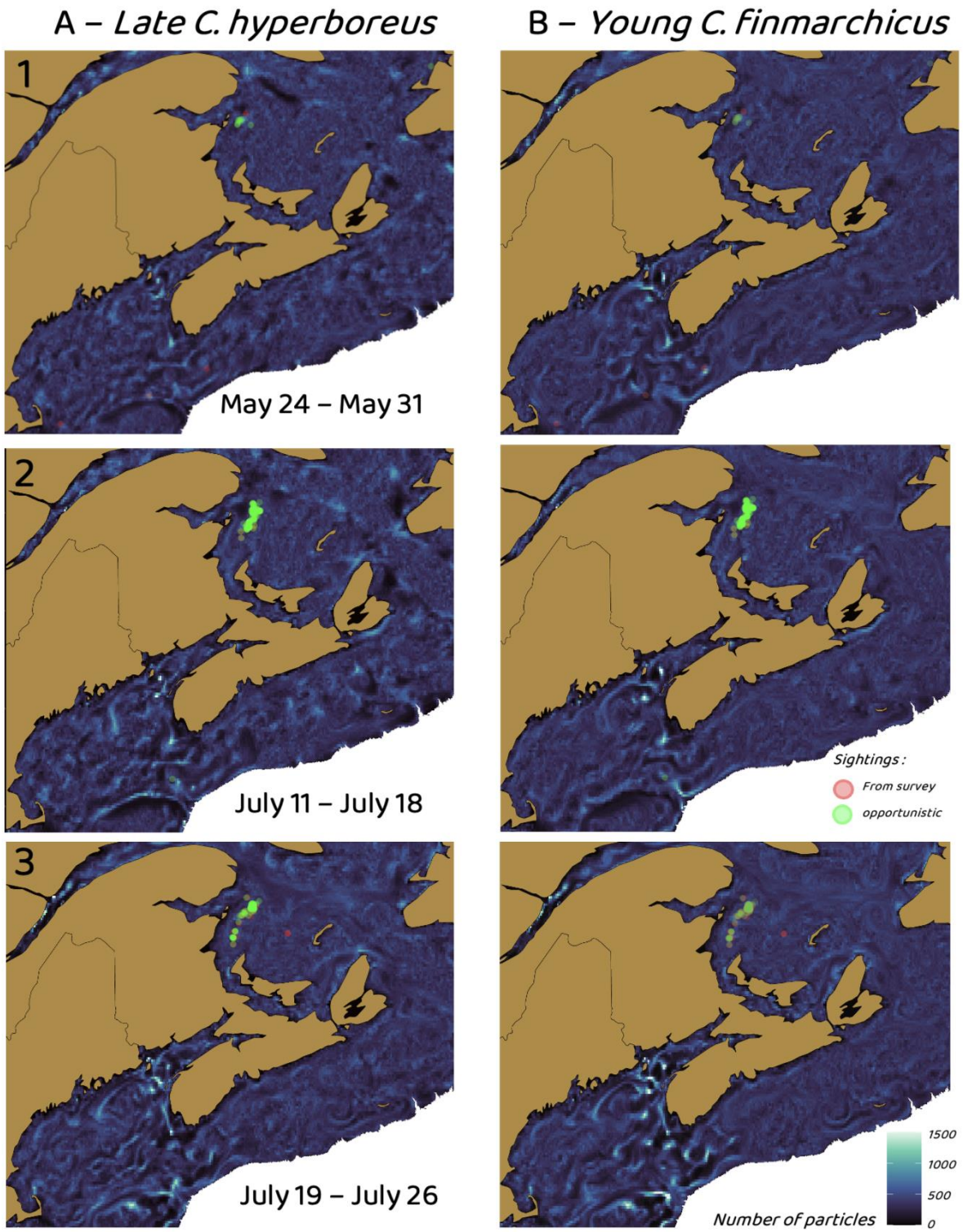

Figure 10. 6 examples of output maps showing the potential aggregation areas of late C. hyperboreus (A) and young C. finmarchicus (B) for different periods of 8 days in 2018. The red and green plots show the sightings from surveys and opportunistic respectively, of the corresponding period.

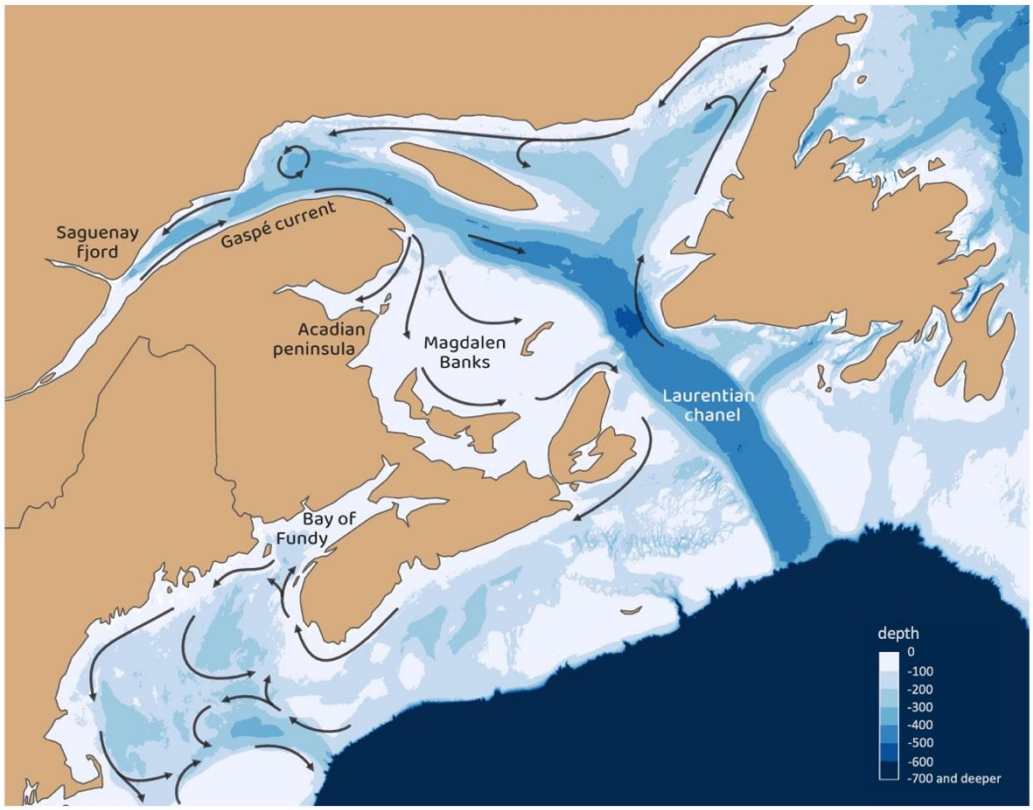

Figure 11. Bathymetry, main surface currents in the study area, and name of the locations mentioned in this report (sources: Sorochan et al., 2021 (A); Woods Hole Oceanographic Institution).

4. Prediction of the suitable habitat of the North Atlantic right whale in its main summer habitat

4.1. Data

4.1.1. Sightings and environmental data

We combined gap-free environmental satellite observation data (i.e. level 4), and sightings from 2017 to 2021 provided at a high spatial resolution (*O* 1 km), leading to a potentially important improvement in models' accuracy.

The sightings data we use come from 1) the North Atlantic Right Whales Consortium (NARWC) sightings database including surveys conducted from the late 1990's to the present and opportunistic sightings as well, and 2) the systematic surveys led by Fisheries and Oceans Canada (DFO) since 2017 (Figure 12). It is noteworthy that presence and absence data in the systematic surveys are strongly imbalanced, the proportion of presence data among all observations being less than 0.5 %.

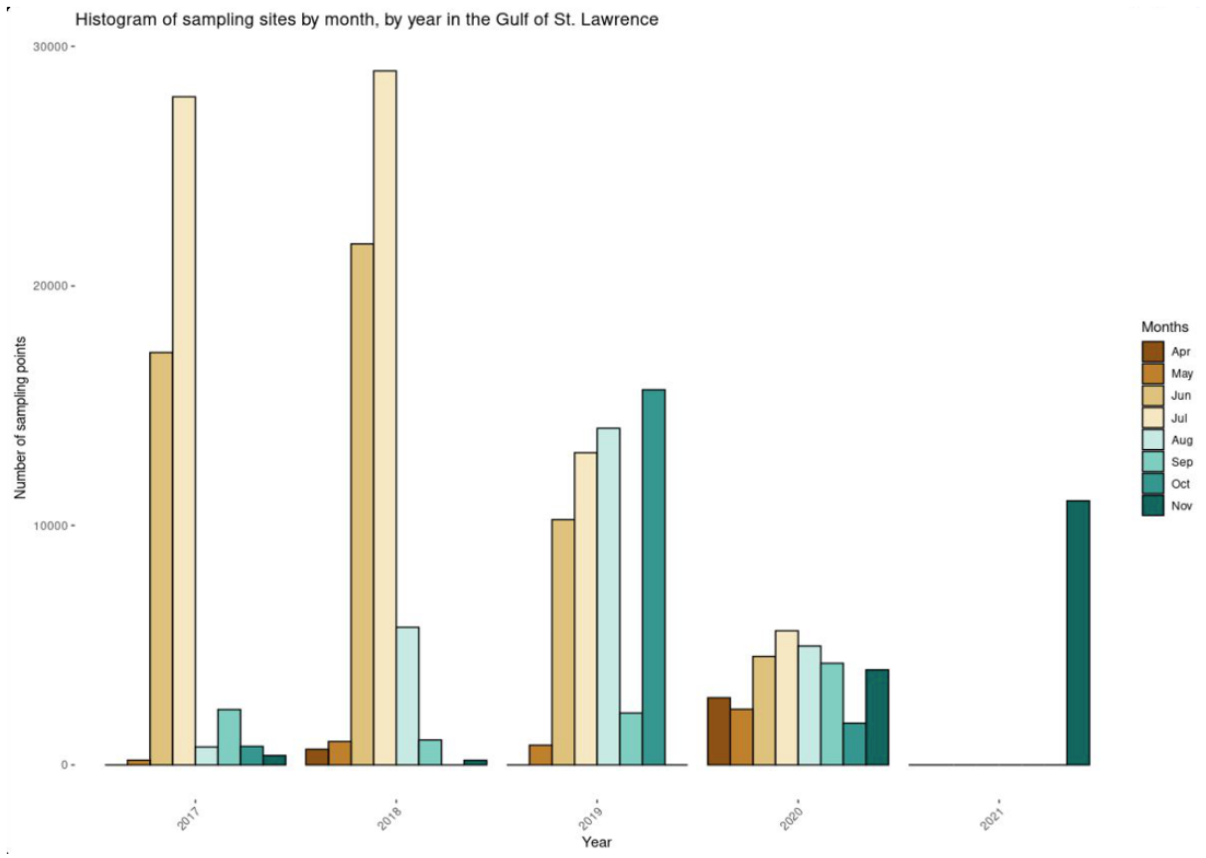

Figure 12. Histogram of the sampling effort of DFO and the NARWC combined from 2017 to 2021 in the Gulf of St. Lawrence (DFO's data are missing for the year 2021).

In total, we have access to both opportunistic detections and sightings from systematic surveys for a period spanning from 2003 to 2021. However, for consistency reasons we chose not to use sightings data from the NARWC *before* 2017 since it is this year that DFO started systematic surveys in the GSL. We also used sightings from the GSL only, since this is the region of interest for the SmartWhales project (Figure 13).

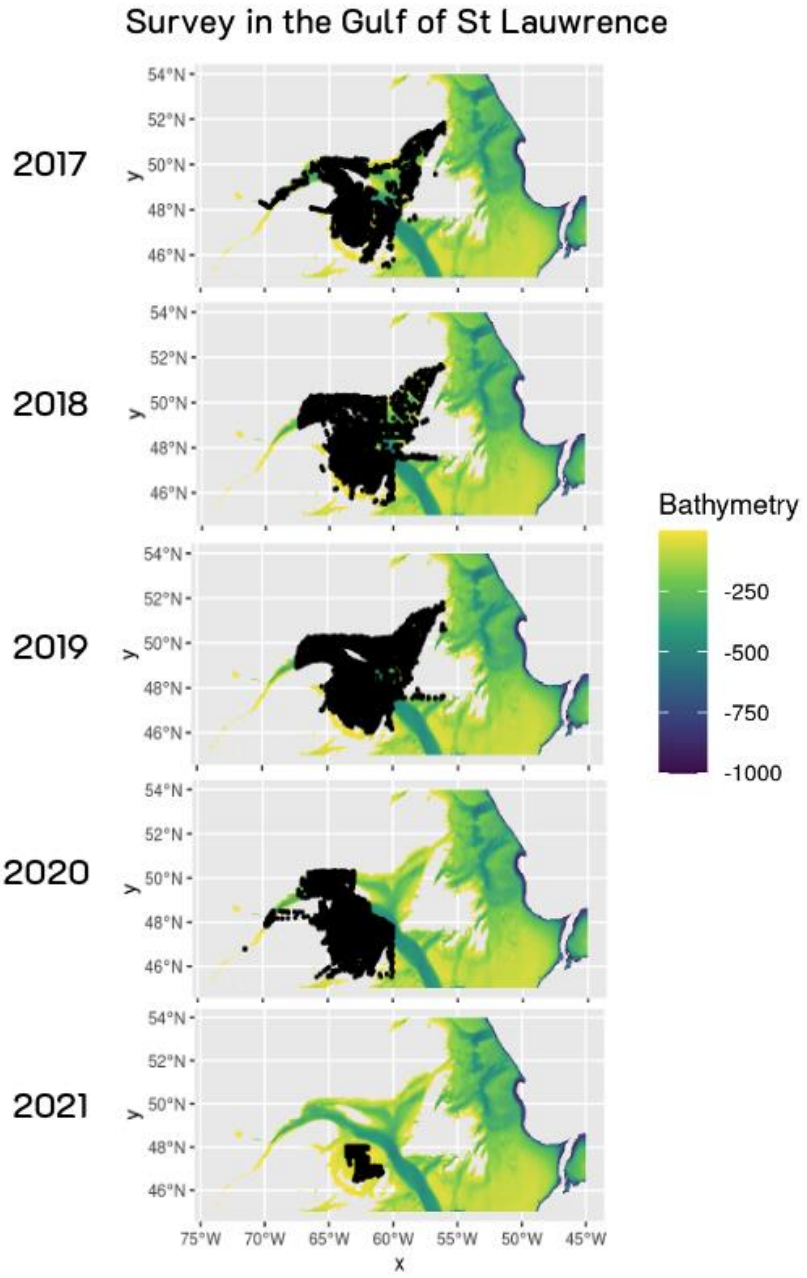

Figure 13. Maps showing sample sites (black points) of DFO and NARW surveys combined in the Gulf of St. Lawrence for the entire summer season.

Environmental variables that were used as explanatory variables for the calibration/training of the SDMs can be classified as *dynamic* (i.e., rapidly changing sea surface properties) or *static* (e.g., bathymetry-derived features), as well as *biological* (e.g. primary production, chlorophyll-*a*) or *physical* (e.g. sea surface temperature, fronts, etc.). These data come from raw satellite remote sensing observations from NASA and ESA (Near Real Time – NRT - level 2) after being processed by Arctus and ACRI-ST to obtain geophysical variables suitable (NRT level 3 and/or 4) for final products (Ocean Colour

Radiometry products, Chlorophyll-*a*, Primary Production etc.) from which data will be extracted as model inputs for the SDMs.

4.2. Methods

4.2.1. Species Distribution Model (SDM)

SDM come in many different sorts that are used to predict either habitat suitability, range, probability of occurrence, as well as density and abundance of cetaceans on regional scales, including the North Atlantic right whales (Pendleton et al., 2012, Ross et al., 2021). These models are based on linear and/or nonlinear statistical relationships between a suite of explaining variables (environmental, climatic, biological data) and species occurrence data (Silber et al., 2017) to predict the species occurrence (Figure 14).

Several studies showed that simultaneously applying several algorithms together, i.e. doing an ensemble modeling approach, lead to generally better predictions of the probability of presence than using a single modelling approach (Araujo & New, 2007; Grenouillet et al., 2011). Ensemble models consist in mapping both main trend (mean, median, etc.) and overall variation (and uncertainty) across all selected models and then selecting a few models satisfying a selection criterion and combining their output. Many algorithms can be used to understand and predict species distribution, like regression-based techniques (Generalized Additive Models, Generalized Linear Models, etc.) or machine learning-based methods (Artificial Neural Network, Classification Tree Analysis, etc.). Ensemble modelling methods combine several of these different methods to predict and project spatial species occurrence.

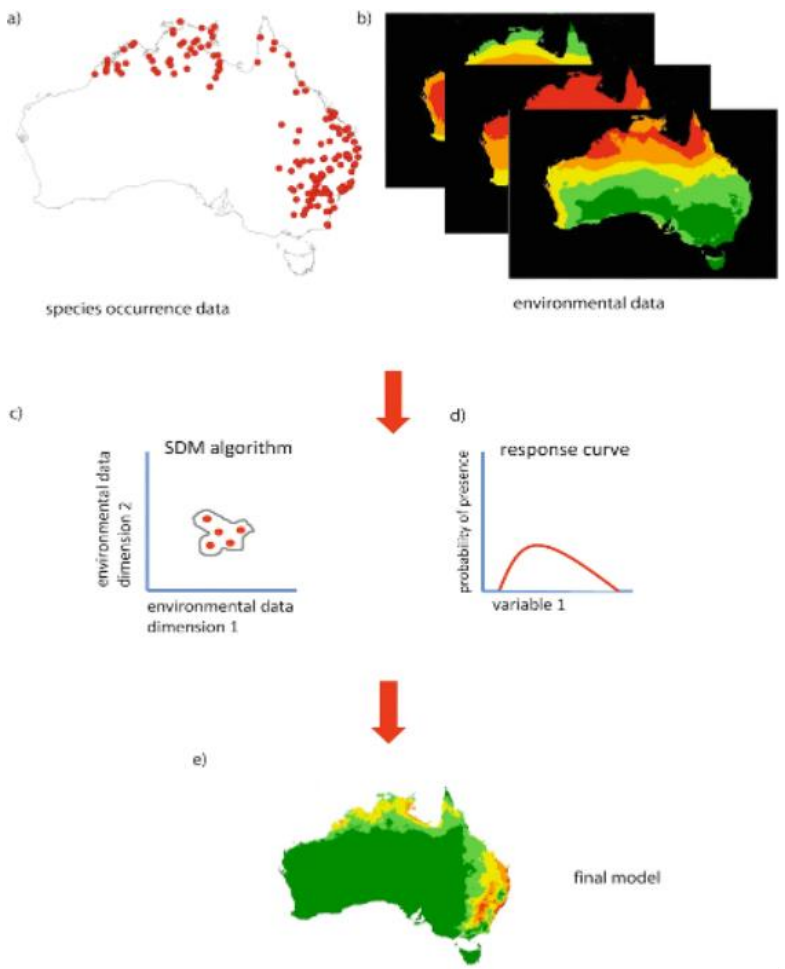

Figure 14. Schematic representation of species distribution modelling process (Segurado & Araujo, 2004)

The overall objective of this project is to forecast NARW distribution in the GSL at a fine spatio-temporal scale. One key challenge is that we will not have access to future projections of the forcing variables we use to best describe right whales' distribution. So, we would like to know whether current environmental conditions may have an influence on the next few days of right whales' distribution. Based on the hypothesis that the right whales' fundamental environmental niche (environmental conditions suitable for their survival, growth and reproduction) has not changed since 2017, we will build an ensemble distribution model and test its predictive capability with past data. **The rationale is to build several SDMs using past data with different temporal lags to the event of occurrence to identify the lag that provides the best trade-off between the accuracy and the lag of the forecasts.**

4.2.2. Data Selection

All the metrics available in NRT have been tested to screen the variables that explain the most information about the distribution of the NARW presence in the GSL. For each variable evaluated, the Pearson's correlation index has been calculated between reference and shuffled predictions (null model). A correlation score between -1 and 1 is returned. The higher the value, the more influence the variable has on the model, while a value of 0 assumes no influence at all the variable on the model. Only the variables showing an importance above 10% have been kept. A Variance Inflation Factor (VIF) has been calculated on the selected variables to test for collinearity between them (the lower the score, the less correlated a variable is with the others).

4.2.3. Models' parameterization

We used extensively the functions from the R package Biomod2 to perform our computations, simulations and post-processing estimations. One linear regression model (GAM) and three machine learning methods (Boosting Regression Tree, Classification Tree Analysis and Random Forest) have been selected for the final ensemble. We chose a k-fold cross validation strategy. The k-fold method splits the original dataset into k datasets (here we chose 4) of equal sizes: each part is used successively as the validation dataset while the other k-1 parts are used for the calibration, leading to k calibration/validation ensembles. This multiple splitting has been repeated 5 times to avoid data sampling bias during the splitting dataset process and to make sure to have different independent validation dataset multiple times, which leads to 84 models being ran in total for each area tested (Figure 15).

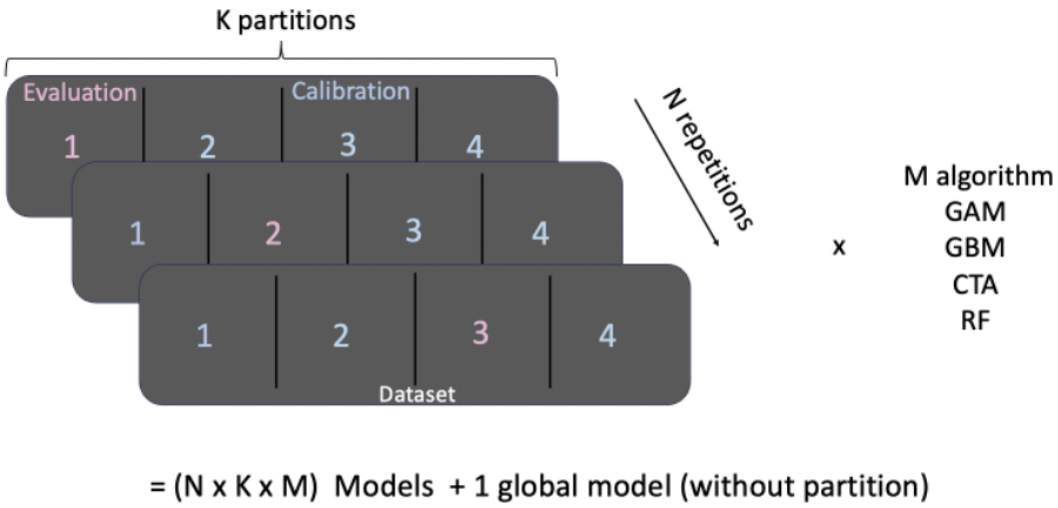

Figure 15. Schematic representation of the partitioning process with the k-fold strategy.

From these models, only the ones with a ROC score above 0.6 and a TSS score above 0.2 are selected. The committee's averaging score is calculated by taking the average of these binary predictions. It follows a simple vote procedure:

- Each single model votes for the species being either present (1) or absent (0).
- The sum of ones is then divided by the number of single models voting.

This measure gives both a prediction and a measure of uncertainty. When the prediction is close to 1 (resp. 0), it means that all models agree to predict a presence (resp. an absence). When the prediction is around 0.5, it means that half the models predict a presence and the other half an absence. The committee averaging is then used to plot the probability of presence that also reflects the uncertainty in the ensemble prediction.

Different metrics and outputs have been calculated to assess the accuracy of the SDM ensemble:

- Calibration and evaluation scores of both ROC and TSS evaluation metrics;
- The absolute percentage of importance for each independent (environmental) variable;
- The response curve of the probability of presence for each independent variable;
- Spatial projections of the probability of presence in response to environmental variables distributions.

4.2.4. Calibration and evaluation scores of ROC and TSS

ROC represents the performance of a binary classification model by ploting the true positive rate against the false positive rate for different classification thresholds. The Area Under the ROC Curve (AUC-ROC) is often used as an overall measure of model performance. The closer AUC-ROC is to 1, the better the model's performance. ROC is particularly useful when classes are imbalanced (i.e., there is an imbalance between positive and negative classes), which is clearly the case here.

TSS is a metric that measures the performance of a binary classification model, considering all possible outcomes, i.e. true positives, true negatives, false positives, and false negatives. It is calculated by subtracting the false positive rate from the true positive rate. TSS ranges from -1 to 1, where 1 represents perfect performance, 0 represents performance equivalent to a random model, and -1 represents completely incorrect performance. TSS is useful for assessing a model's ability to discriminate between positive and negative classes.

In summary, ROC and TSS are two commonly used metrics to evaluate the performance of binary classification models. ROC focuses on the trade-off between true positive and false positive rates, while TSS considers a broader set of measures to assess model performance.

4.2.5. Absolute percentage of importance of each environmental variable

For each variable to be evaluated, the Pearson’s correlation index has been calculated between reference and shuffled predictions. A correlation score between -1 (high negative correlation) and 1 (high positive correlation) is returned. The higher the absolute value, the more influence the variable has on the model, while a value of 0 assumes no influence at all on the model. Five repetitions have been done for each variable tested.

4.2.6. The response curve of the probability of presence for each variable

The response curves show the sensitivity of the model to the studied variable. This function is an adaptation of the Evaluation Strip method proposed by Elith et al. (2005). To build the predicted response curves, we do as follow:

- *n-1* variables are set constant to a fixed value;
- The remaining variable is varied throughout its range;
- Predicted values are computed for each combination possible.

4.2.7. Probability of presence predictions

At the outset of this process, we have identified which variables give the most information about NARW distribution and which algorithms and parameters allow for the best performance and projections of habitat suitability. Then, we can explore the information that past variable could give to the system. As previously mentioned, the idea is to see whether the inertia in the system is sufficient to allow the use of lagged environmental variables values to explain future right whale occurrences: instead of using the information of the environmental variables at the day of observed presence or absence, we will train the model with lagged 8-day periods of environmental variables. For example, if the date of the occurrence event is the 20th of June, the model will be trained with the value of each environmental variable at this same location of the 12th of June (Figure 16). If this procedure shows predictive power, it means that we could predict NARW distribution probability 8 days ahead of time with current environmental data.

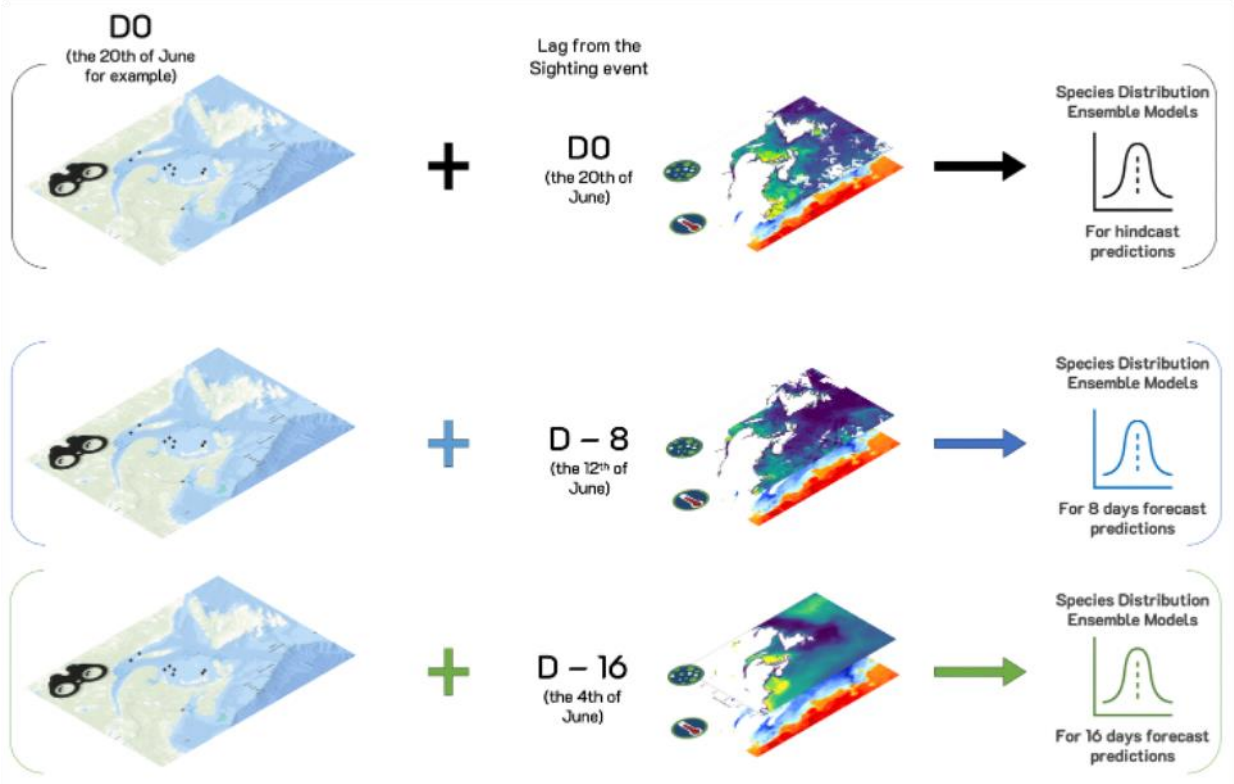

Figure 16. Schematic representation of the concept of using lagged environmental variables.

Furthermore, environmental variables are available at three different temporal resolutions: daily, every 8 days, or monthly. We opted for 8-day periods, since daily observations are difficult to interpolate spatially (cloud/ice presence, etc.) and failed to capture the typical behaviour of NARW that tend to stay in the same location for an average of 10 days (Davis, G., 2023). We also sought greater precision than monthly predictions. We tested increasing lags following the assumption that the further we go back in time, the less predictive power the model will have (Figure 17).

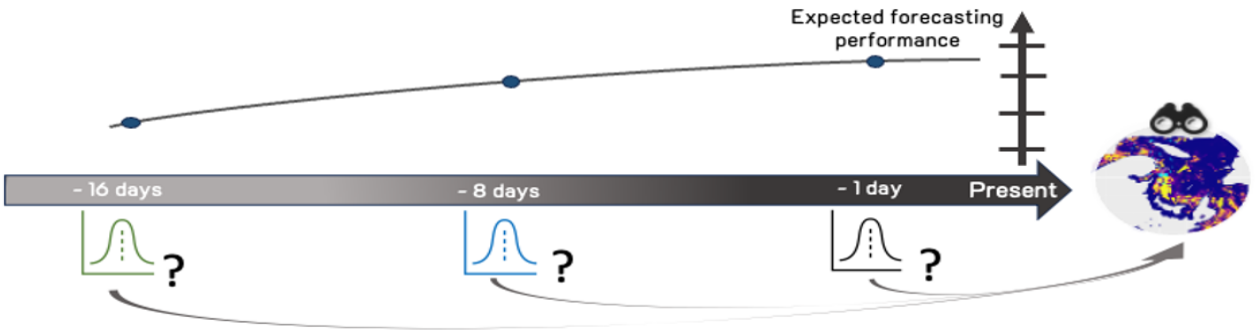

Figure 17. Schematic representation of the expected models' forecasting performance depending on the chosen lagged in time.

4.3. Results and discussion

4.3.1. Environmental variables selection

Two variables showed an absolute percentage of importance less than 10% and have been excluded: Colored Detrital Matter (CDM) and Particulate Backscattering coefficient (BBP). The following variables have been kept: SST, PAR, Chl-a, PP and Bathymetry. The Variance Inflation Factor analysis showed that there was no problematic collinearity between these variables.

4.3.2. Models' parametrization

The ROC and TSS metrics have been calculated for the ensemble model on the calibration (training) and evaluation steps (test on an independent dataset). Evaluation scores were satisfactory for both the training and evaluation steps (Figure 18).

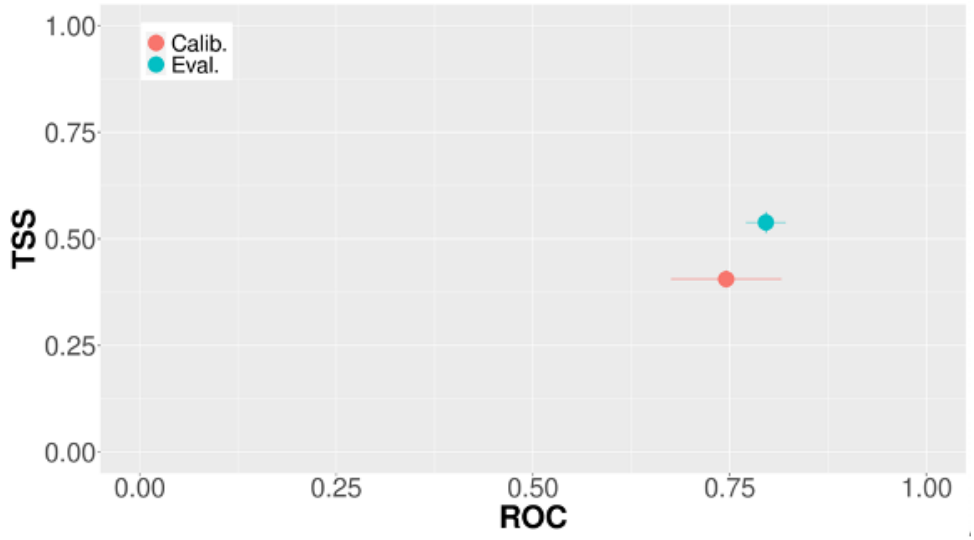

Figure 18. ROC and TSS evaluation scores for the calibration and evaluation steps of the ensemble model.

Bathymetry emerges as the most influential variable, accounting for almost 60% of absolute importance (Figure 19). This could be attributed to the fact that NARW typically feed in the first 200 m, and there are pronounced bathymetric discontinuities in the GSL. Additionally, bathymetry remains constant over time, providing algorithms a

stable parameter to capture recurrent patterns in NARW distribution, thereby assigning greater weight to this variable.

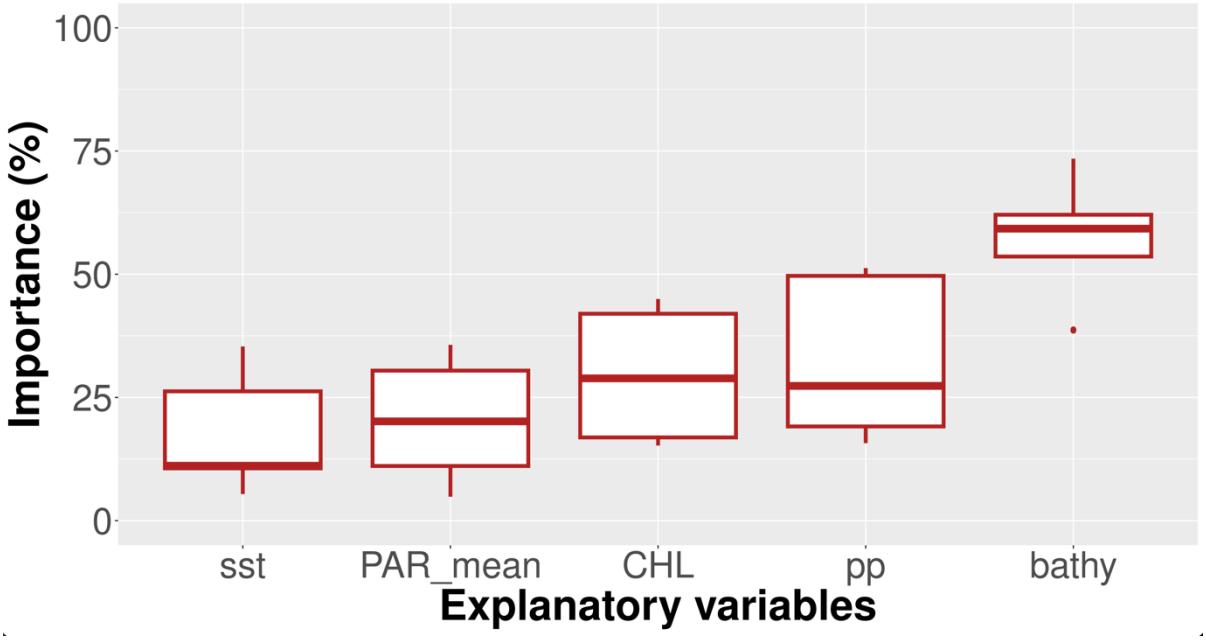

Figure 19. Boxplot of the absolute percentage of variable importance of the ensemble model.

The remaining four variables can be grouped into two categories: SST and PAR (physical variables) each contribute less than 20%, while Chl-a and PP (biological processes) contribute both for 30%. Primary production rate presented higher temporal variability and are likely to better reflect the nature of the NARW trophic environment.

NARW have a higher likelihood of presence between 0°C and 10°C, and around 15°C as well. They also exhibit a preference for low Chl-a concentrations, but a contrasting affinity for relatively high levels of PP. They also seem to aggregate at two distinct bathymetry levels: shallow areas and above 400 m deep parts, typical of the Laurentian channel and slope areas.

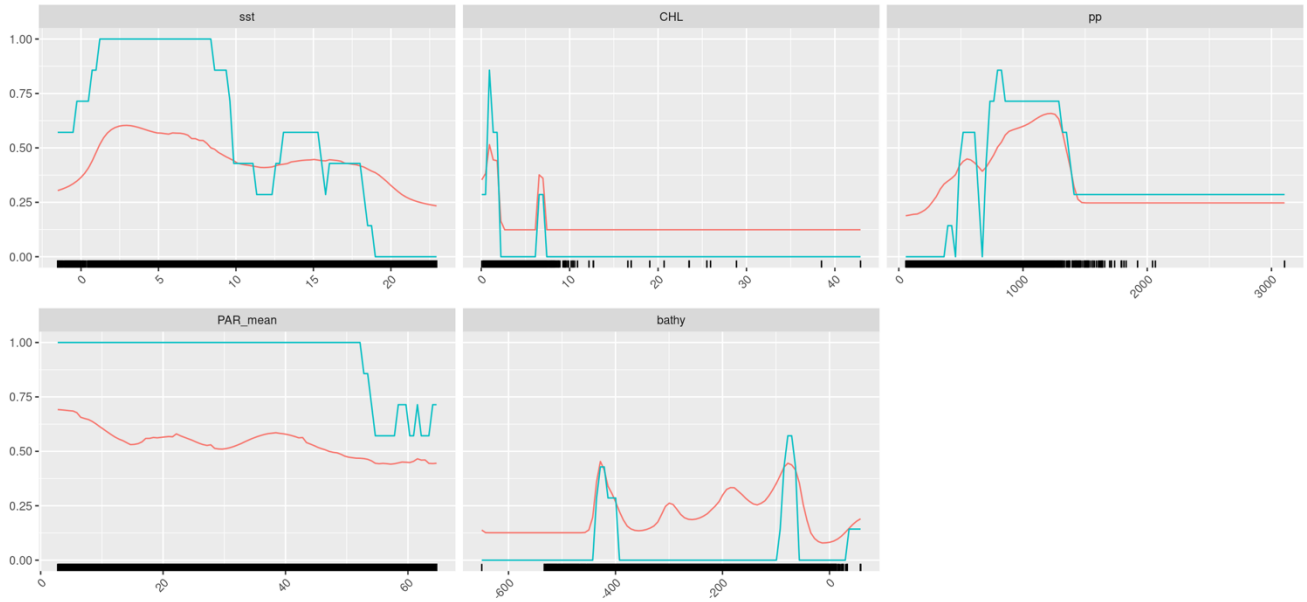

Figure 20. Response curves of NARW probability of presence for each independent variable. The Y axis shows the probability of presence, and the X axis is the unit of each variable. The red and blue curves represent two different ensemble modeling procedures: red and blue curves represent two different ensemble modeling procedures: red is the mean probability of each model in the ensemble; blue is the committee averaging of the single models.

However, both ensemble procedures diverge slightly for this variable: the GM procedure leads to a more continuous influence of bathymetry than the sharp bimodal influence revealed by the SLM. The responses are even more contrasted for PAR: with the GM, the probability of presence remains constantly low, while the SLM indicates a high probability of presence for PAR values between 0 and 50, that is dropping rapidly above this value. These differences could reflect the lower predictive power of these variables.

4.3.3. Projection of the probability of presence of NARW in the GSL in summer

The projection of habitat suitability (we use this term interchangeably with the probability of NARW presence) was computed for each 8-day period by training the models of the systematic sampling conducted in the GSL from April to November of 2020. The aim was to visualize the predictions from the SLM ensemble model, compare them with actual sightings, and assess their accuracy in relation to sampling efforts (Figure 12 and Figure 13).

The prediction quality varies with the season, exhibiting higher accuracy early in spring (Figure 21-A to Figure 21-D) than in early autumn (Figure 21-E; Figure 21-F).

Accuracy is also influenced by sampling efforts and the zone coverage. SDM may predict suitable zones that have not been sampled, such as the head of the St Lawrence maritime estuary off Tadoussac, and further along the north shore of the estuary between Baie Comeau and Les Escoumins (Figure 21). These areas frequently report opportunistic sightings, but supporting systematic surveys data are very limited there (e.g. Figure 21-E).

It is important to note that NARW are so few in the ecosystem (about 300) that the probability that no NARW is sighted in an area predicted to represent a favorable habitat remains high, even if the SDM is accurate (e.g. Figure 21-A). Conversely, an accurate SDM should lead to a low frequency of actual NARW sightings located within areas predicted to be unfavorable, except for the rare occurrence of NARW transiting between favorable areas via regions of low interest for them (e.g. the Laurentian channel, Figure 21-A; Figure 21-C). Spatial resolution plays a role, where opportunistic sightings were observed at the head of the Laurentian channel, an area generally predicted as suitable by the SDM, but not this time (Figure 21-E).

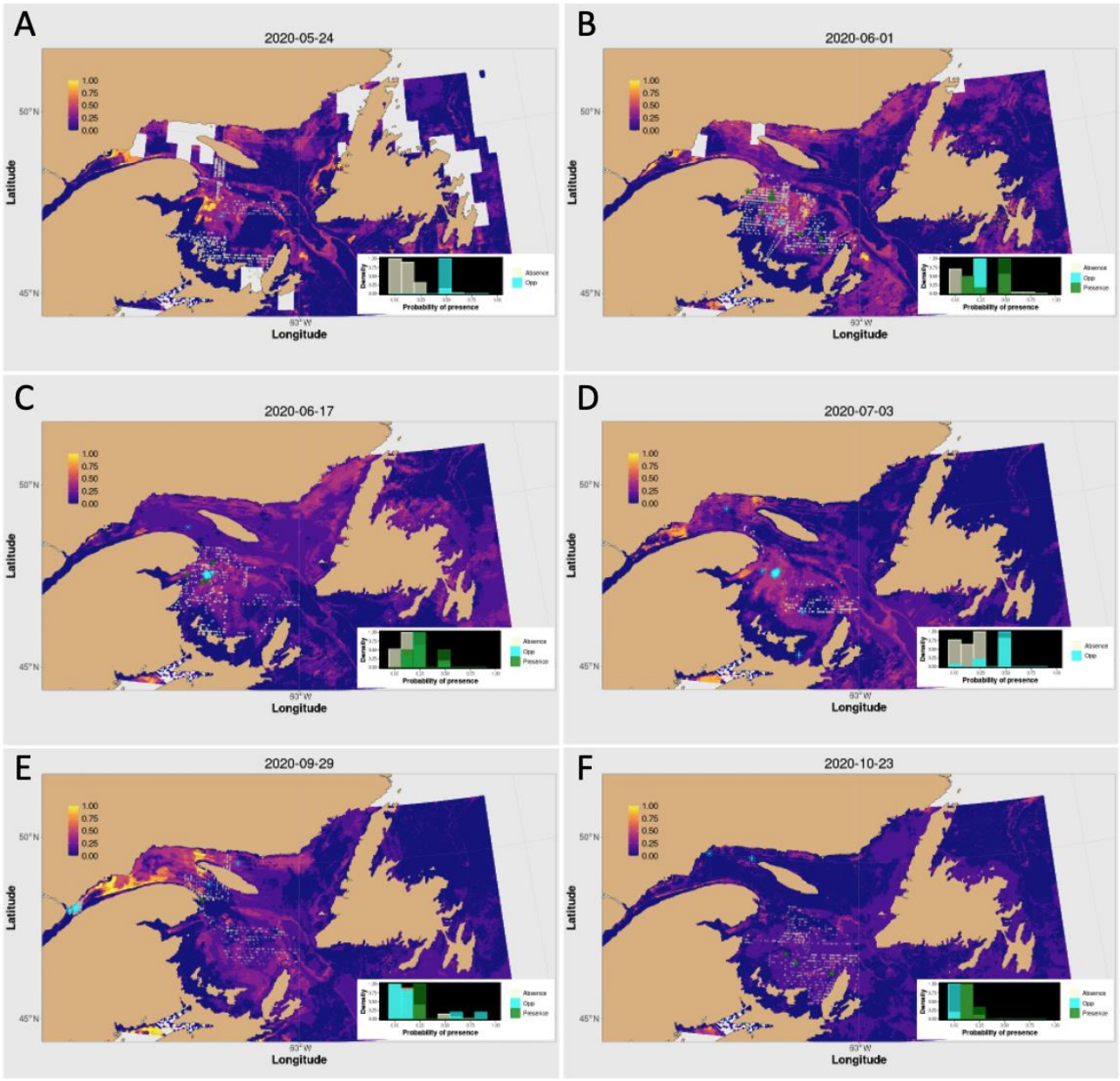

Figure 21. Examples of prediction maps of NARW habitat suitability in the GSL for 2020, classified by date, with an example each period of the summer season. Values range from 0 (non suitable) to 1 (highly suitable). White dots represent the positions of recorded absence during the systematic sampling; green crosses are recorded NARW presence during the same systematic surveys; light blue crosses are opportunistic sightings (presence from non-systematic surveys). The histograms represent the frequency distribution of the simulated probability of presence at each observation location (presence and absence). Absence points should be predicted with low probability of presence (true negative), while blue and green point should correspond to high probability of presence (true positive), and hence be found on the right-hand side of this graph.

4.3.4. Predictions based on lagged environmental variables

In order to compare the models based on lagged environmental variables with the initial regional model, we computed the same outputs and metrics (ROC & TSS), the absolute importance of each variable, the response curve and projections for both models, based on 8 days lagged environmental variables (Model –8 days) and on 16 days lagged (Model –16 days). Unfortunately, due to lack of time and the computational resources it takes, we didn't have time to compute the ensemble model but single models have been run.

In this numerical experiment, the ROC & TSS values remained reasonably high for both lags of – 8 and – 16 days in forcing variables (Figure 22) .

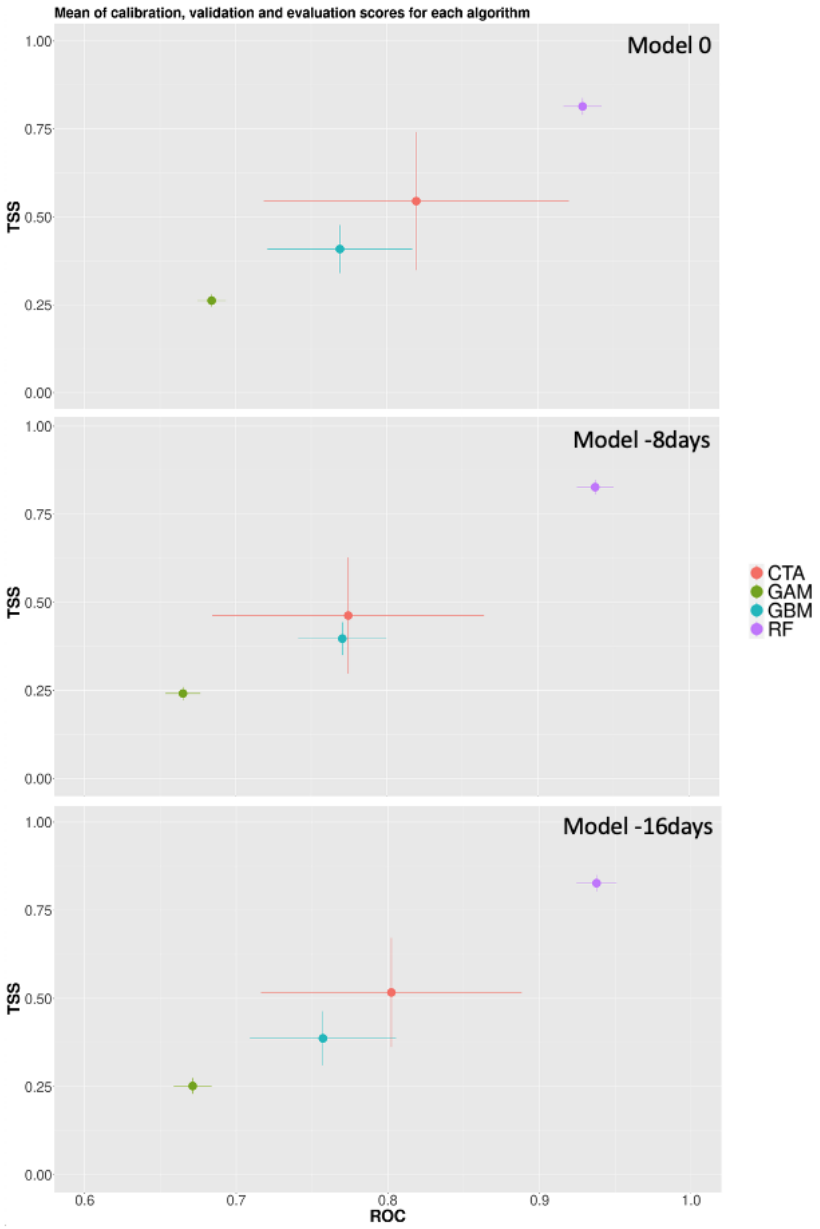

Figure 22. Comparison of ROC and TSS scores between the initial model based on variables at the date of the sightings (Model 0), the -8days Model and the -16days Model (the X axis starts at 0.6).

After a lag of – 16 days, the bathymetry remains the most influencing variable, which is expected since this one is *not* varying in time. Interestingly though, chlorophyll-a concentration retains a fairly high explanatory power even after this period of time, suggesting that some inertia remains in the system that could help explaining the future distribution of NARW based on recent past environmental conditions. Here we showed the example of 2 algorithms, CTA and GBM that are the 2 medium models if we refer to evaluation scores. Taking these 2 models allow to have an idea of average results as the goal is to build an ensemble model based on these 4 algorithms (as made for the Model 0).

Model – 8 days

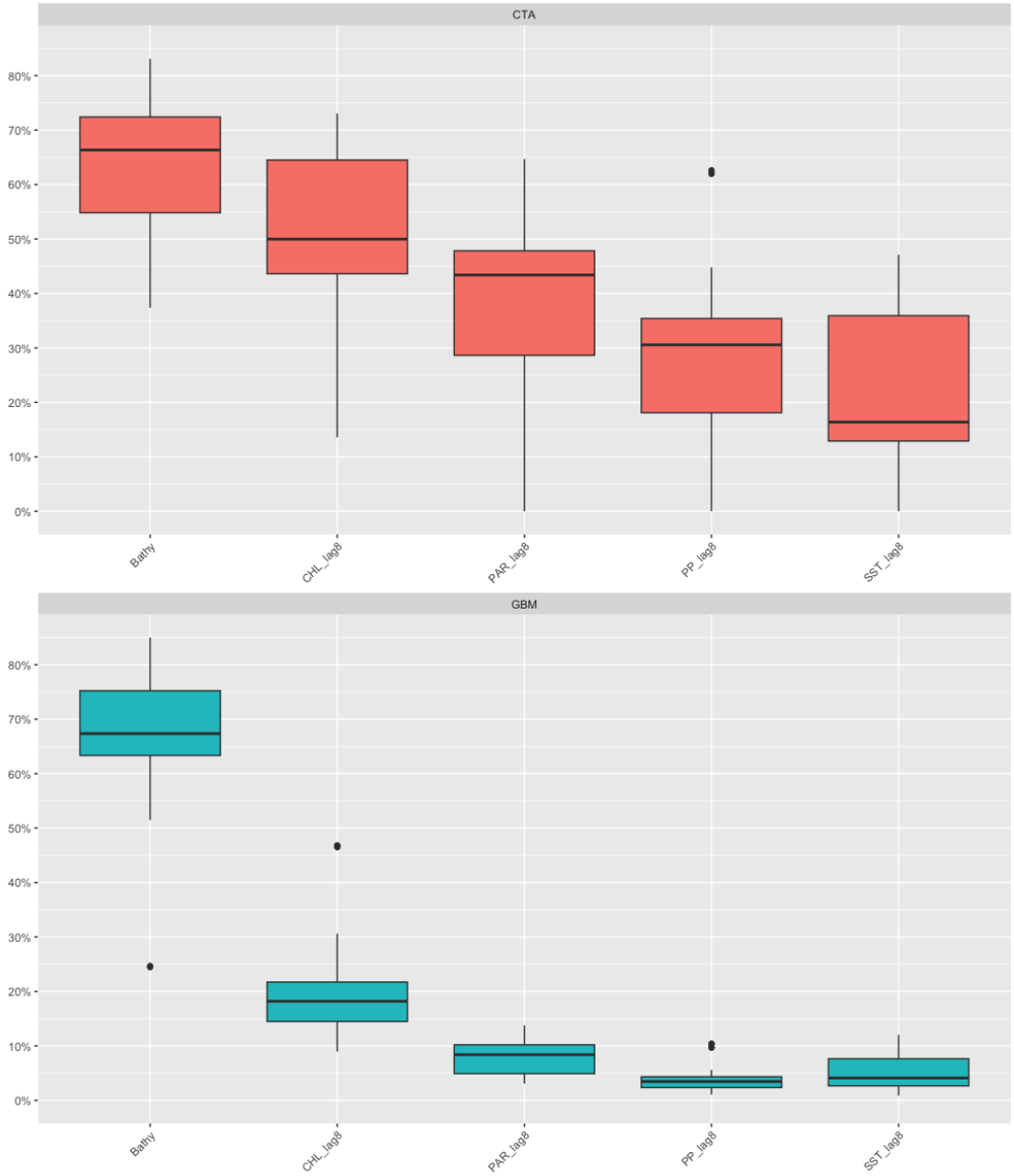

Figure 23. Boxplot of the absolute percentage of variable importance of CTA (top) and GBM (bottom) algorithm based on variables with a lag of -8days.

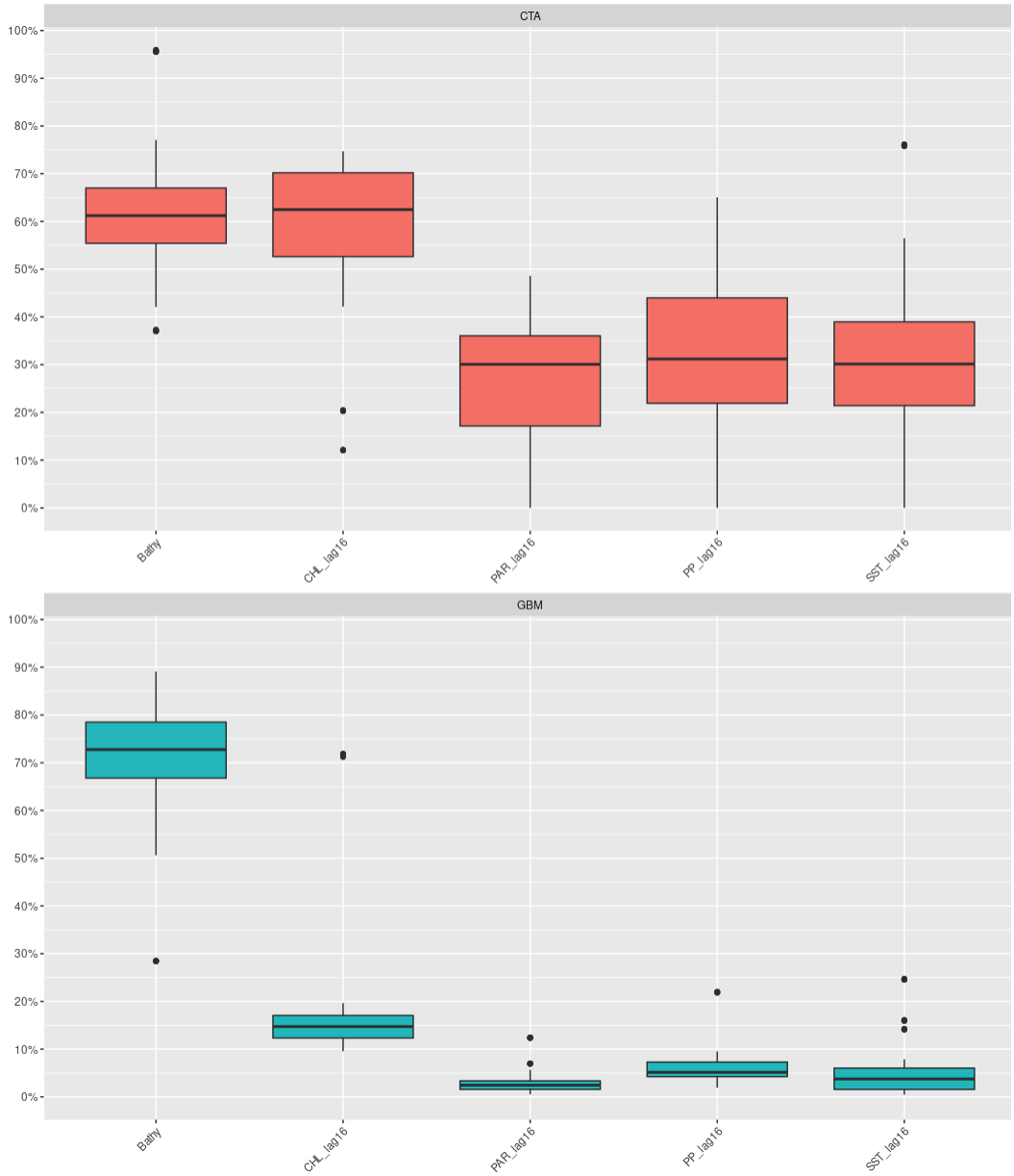

Figure 24. Boxplot of the absolute percentage of variable importance of CTA (top) and GBM (bottom) algorithm based on variables with a lag of -16days.

- **Projections**

Thanks to projecting predictions, we are allow to have a better idea of the ability of models to discriminate true/false presences and true/false absences. The next panel (Figure 25) of 5 maps shows the predictions of the Models -8days for 2 periods, 2020-05-24, and 2020-07-11, for CTA and GBM.

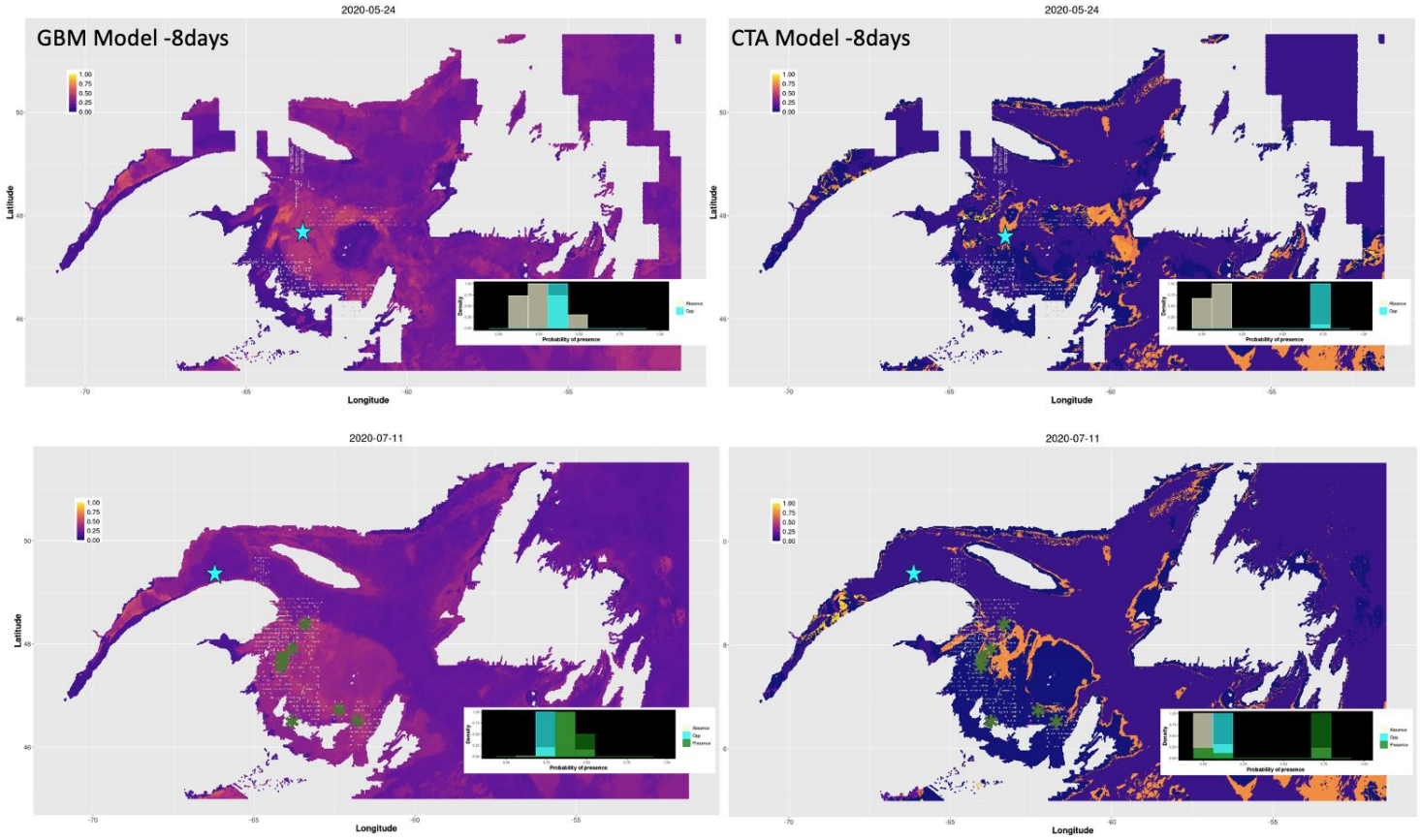

Figure 25. Projections of the predicted habitat suitability of CTA Models -8days (right) and GBM Models -8days (left) for the week 2020-05-24 (top) and the week 2020-07-11 (bottom), in the Gulf of St. Lawrence.

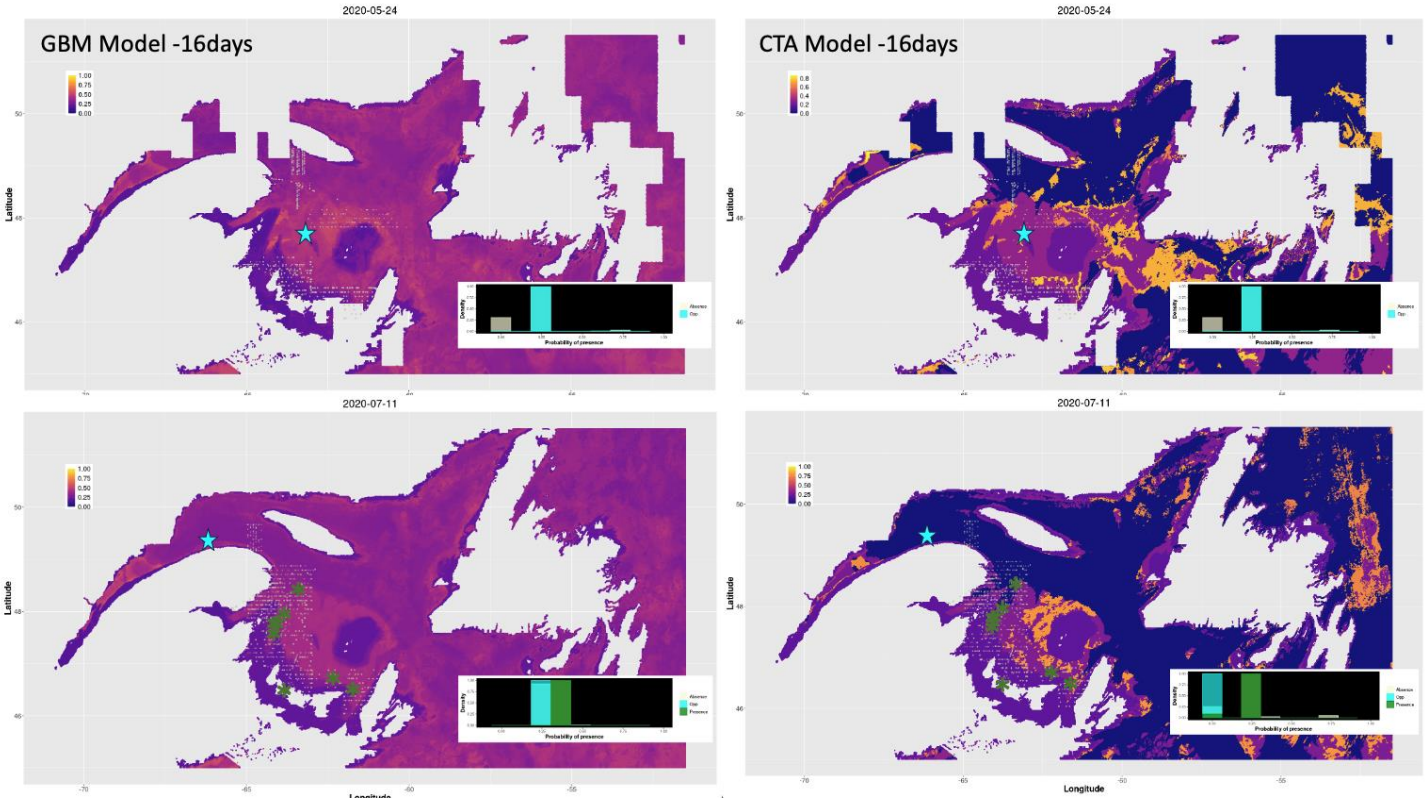

Figure 26. Projections of the predicted habitat suitability of CTA Models -16days (right) and GBM Models -16days (left) for the week 2020-05-24 (top) and the week 2020-07-11 (bottom), in the Gulf of St. Lawrence.

If we compare both Models-8days and Models-16days (for both CTA and GBM algorithms), we can see that using -8days variables allow to better discriminate true/false presences and true/false absences. Indeed, absences seem to be more predicted with low suitability and presences with higher suitability.

Mirroring both algorithms (CTA and GBM) underline the meaning of computing and using an ensemble model for forecasting habitat suitability. Here is a really good example to illustrate this concept, as we can see that GBM is really smooth in the predictions while CTA is way sharper. Combining both allow to minimize the bias linked to each algorithm and combine different approaches that may catch complementary signals.

These are very preliminary results of using past data to forecast habitat suitability of right whales in the GSL. We think that computing ensemble models and projecting the all summer season for each year of data will allow to get a better oversee and make decisions about the possibility of using one of the models to forecast NARW suitable habitat in the GSL.

5. Perspectives

The 8-day period projection of habitat suitability reveals distinct patterns and clear seasonal trends in the distribution of NARW in the GSL. To further improve our

understanding of the NARW use of their environment in summer in the GSL and enhance the predictive power of the SDM, we propose several actions.

While absences are generally well predicted, including information on the areas of dense aggregation of NARW preferred prey is expected to improve the SDM performance for predicting presences at a spatio-temporal scale that should reflect realistic trophic processes. This information can be computed now thanks to the recent advance in the simulation of the interaction between the vertical behavior of the NARW preys and the circulation in the GSL.

Some work remains to be done to translate these numerical results into layers of input for the SDM, but it will be done soon after the term of this project. We will also incorporate non-systematic sightings to add more information during the SDM training process. The key element here is to generate pseudo-absences based on the opportunistic presence reported.

As shown by the projections of habitat suitability during 2020 (Figure 21), training seasonals models could improve NARW habitat suitability predictions. Spring is a productive season during which several of the independent variables used to force the SDM are likely to reflect the intense biological activity the NARW rely on to feed (e.g. Chl-a, PP). However, from midsummer onward when the GSL biological activity is less intense (post-bloom period and copepods entering diapause at depth), predicting suitable habitat becomes more challenging (Figure 21-E; Figure 21-F). Training season-specific models could improve their predictive power.

Since the number of whales is given in the sightings database, *density* analysis would be interesting to explore to know more about NARW ecology and behaviour. Whales are social mammals and usually forage in groups. Knowing more about their tendency to stay together or to stray by themselves into different territories and understanding what drivers could influence this behaviour could help decision-makers in managing protected areas.

In the same line of thought, spatial and temporal autocorrelation are key features that could give precious information. Since we have in some instances daily data of NARW occurrences, considering their previous location could guide our predictions. If different areas present the same suitability index but NARW are concentrated in one of them, we hypothesize that they would preferably forage in the vicinity and not swim far away as

long as their current environment remain suitable enough (Optimal Foraging Strategy, Emlen, 1966; MacArthur & Pianka, 1966).

Regarding our exploration of past data to predict the presence of NARW in suitable habitats in the near future (Figure 22 to Figure 26), each environmental variable might have a different temporal dynamic. Hence it will be important to test each combination of lag/variables to see which one would be the most informative at which time horizon.

Finally, while the demonstration of the SDM performance in this report only shows results for 2020, similar analyses will be conducted for the years 2017 to 2019 and 2021 to reveal interannual variability and assess the ensemble SDM robustness. This information about potential suitable habitat for NARW in the GSL could help guiding surveying efforts by DFO into regions that may have been neglected until now owing to our lack of knowledge of the complex behaviour of the NARW since they have started to exploit the GSL more intensively by the mid 2010s.

6. Conclusion

We developed and implemented an approach that could make use of satellite-derived products generated by SIMBA in the context of smarthwhales. The *Calanus* spp distribution model output is missing in the current iteration of the SDM ensemble, but it will be integrated into it in the near futur (see above).

We will also explore the performance of SDM ensembles forced by lagged environmental data to make short time predictions (a horizon of a few weeks) of NARW distribution in its summer habitat. The very high spatial resolution and temporal coverage of the satellite data generated in NRT by WP2 represent a clear added value to this approach, that has never been used yet at this scale, to our knowledge. Using NRT variables to predict species distribution is an innovative way to meet SIMBA's project objectives.

Throughout the process, we could provide feedback about remote sensing output and copepod models and develop a concerted workflow between satellite-derived data, right whales' prey simulated distribution, and SDMs output and indices to communicate to the end-users.

References

Akyuz, F.A., Kandel, H., Morlock, D., 2017. Developing a growing degree day model for North Dakota and Northern Minnesota soybean. Agric. For. Meteorol. 239, 134–140. https://doi.org/10.1016/j.agrformet.2017.02.027

Araujo, M., & New, M. (2007). Ensemble forecasting of species distributions. *Trends in Ecology & Evolution*, *22*(1), 42–47. https://doi.org/10.1016/j.tree.2006.09.010

Baumgartner, M., Cole, T., Campbell, R., Teegarden, G., Durbin, E., 2003. Associations between North Atlantic right whales and their prey, Calanus finmarchicus, over diel and tidal time scales. Mar. Ecol. Prog. Ser. 264, 155–166. https://doi.org/10.3354/meps264155

Baumgartner, M., Mate, B., 2003. Summertime foraging ecology of North Atlantic right whales. Mar. Ecol. Prog. Ser. 264, 123–135. https://doi.org/10.3354/meps264123

Baumgartner, M., Wenzel, F., Lysiak, N., Patrician, M., 2017. North Atlantic right whale foraging ecology and its role in human-caused mortality. Mar. Ecol. Prog. Ser. 581, 165–181. https://doi.org/10.3354/meps12315

Baumgartner, M.F., Mayo, C.A., Kenney, R.D., 2009. Enormous Carnivores, Microscopic Food, and a Restaurant That's Hard to Find, in: The Urban Whale: North Atlantic Right Whales at the Crossroads. Harvard University Press, Cambridge, Mass., pp. 138–171.

Beardsley, R.C., Epstein, A.W., Chen, C., Wishner, K.F., Macaulay, M.C., Kenney, R.D., 1996. Spatial variability in zooplankton abundance near feeding right whales in the Great South Channel. Deep Sea Res. Part II Top. Stud. Oceanogr. 43, 1601–1625. https://doi.org/10.1016/S0967-0645(96)00050-1

Bouchard, B., Barnagaud, J.-Y., Poupard, M., Glotin, H., Gauffier, P., Torres Ortiz, S., Lisney, T.J., Campagna, S., Rasmussen, M., Célérier, A., 2019. Behavioural responses of humpback whales to food-related chemical stimuli. PLOS ONE 14, e0212515. https://doi.org/10.1371/journal.pone.0212515

Brennan, C.E., Maps, F., Gentleman, W.C., Lavoie, D., Chassé, J., Plourde, S., Johnson, C.L., 2021. Ocean circulation changes drive shifts in Calanus abundance in North Atlantic right whale foraging habitat: A model comparison of cool and warm year scenarios. Prog. Oceanogr. 197, 102629. https://doi.org/10.1016/j.pocean.2021.102629

Checkley, D. M., R. E. Davis, A. W. Herman, G. A. Jackson, B. Beanlands, L. A. Regier. 2008. Assessing plankton and other particles in situ with the SOLOPC. Limnology and Oceanography 53(5): 2123-2136.

Cheridito, P., Kawaguchi, H., Maejima, M., 2003. Fractional Ornstein-Uhlenbeck processes. Electron. J. Probab. 8. https://doi.org/10.1214/EJP.v8-125

Daase, M., Berge, J., Søreide, J.E., Falk-Petersen, S., 2021. Ecology of Arctic Pelagic Communities, in: Thomas, D.N. (Ed.), Arctic Ecology. Wiley, pp. 219–259. https://doi.org/10.1002/9781118846582.ch9

Davis, G E., Tennant, S C., Van Parijs, S M., Upcalling behaviour and patterns in North Atlantic right whales, implications for monitoring protocols during wind energy development, *ICES Journal of Marine Science*, 2023;, fsad174, https://doi.org/10.1093/icesjms/fsad174

Davies, K., Ross, T., Taggart, C., 2013. Tidal and subtidal currents affect deep aggregations of right whale prey, Calanus spp., along a shelf-basin margin. Mar. Ecol. Prog. Ser. 479, 263–282. https://doi.org/10.3354/meps10189

Davies, K., Brown, M., Hamilton, P., Knowlton, A., Taggart, C., & Vanderlaan, A. (2019). Variation in North Atlantic right whale *Eubalaena glacialis* occurrence in the Bay of Fundy, Canada, over three decades. *Endangered Species Research*, *39*, 159–171. https://doi.org/10.3354/esr00951

Dawson, J.K., 1978. Vertical distribution of *Calanus hyperboreus* in the central Arctic Ocean1: Arctic Ocean *Calanus*. Limnol. Oceanogr. 23, 950–957.

https://doi.org/10.4319/lo.1978.23.5.0950

Dezutter, T., Lalande, C., Dufresne, C., Darnis, G., Fortier, L., 2019. Mismatch between microalgae and herbivorous copepods due to the record sea ice minimum extent of 2012 and the late sea ice break-up of 2013 in the Beaufort Sea. Prog. Oceanogr. 173, 66–77. https://doi.org/10.1016/j.pocean.2019.02.008

Doniol-Valcroze, T., Berteaux, D., Larouche, P., Sears, R., 2007. Influence of thermal fronts on habitat selection by four rorqual whale species in the Gulf of St. Lawrence. Mar. Ecol. Prog. Ser. 335, 207–216. https://doi.org/10.3354/meps335207

Durbin, E., Runge, J., Campbell, R., Garrahan, P., Casas, M., Plourde, S., 1997. Late fall-early winter recruitment of Calanus finmarchicus on Georges Bank. Mar. Ecol. Prog. Ser. 151, 103–114. https://doi.org/10.3354/meps151103

Emlen, J. M. (1966). The role of time and energy in food preference. *The American Naturalist*, *100*(916), 611–617. https://doi.org/10.1086/282455

Fasick, J.I., Baumgartner, M.F., Cronin, T.W., Nickle, B., Kezmoh, L.J., 2017. Visual predation during springtime foraging of the North Atlantic right whale (*Eubalaena glacialis*). Mar. Mammal Sci. 33, 991–1013. https://doi.org/10.1111/mms.12417

Fields, D.M., Shema, S.D., Browman, H.I., Browne, T.Q., Skiftesvik, A.B., 2012. Light Primes the Escape Response of the Calanoid Copepod, *Calanus finmarchicus*. PLoS ONE 7, e39594. https://doi.org/10.1371/journal.pone.0039594

Fortune, S., Trites, A., Mayo, C., Rosen, D., Hamilton, P., 2013. Energetic requirements of North Atlantic right whales and the implications for species recovery. Mar. Ecol. Prog. Ser. 478, 253–272. https://doi.org/10.3354/meps10000

Gaardsted, F., K. S. Tande, and S. L. Basedow. 2010. Measuring copepod abundance in deepwater winter habitats in the NE Norwegian Sea: Intercomparison of results from laser optical plankton counter and multinet. Fisheries Oceanography 19(6): 480-492.

Galbraith, P.S., Larouche, P., Chassé, J., Petrie, B., 2012. Sea-surface temperature in relation to air temperature in the Gulf of St. Lawrence: Interdecadal variability and long-term trends. Deep Sea Res. Part II Top. Stud. Oceanogr. 77–80, 10–20. https://doi.org/10.1016/j.dsr2.2012.04.001

Gavrilchuk, K., Lesage, V., Fortune, S., Trites, A., Plourde, S., 2021. Foraging habitat of North Atlantic right whales has declined in the Gulf of St. Lawrence, Canada, and may be insufficient for successful reproduction. Endanger. Species Res. 44, 113–136. https://doi.org/10.3354/esr01097

Gavrilchuk, K., Lesage, V., Fortune, S., Trites, A.W., 2020. A mechanistic approach to predicting suitable foraging habitat for reproductively mature North Atlantic right whales in the Gulf of St. Lawrence. DFO Canada.

Genin, A., Jaffe, J.S., Reef, R., Richter, C., Franks, P.J.S., 2005. Swimming Against the Flow: A Mechanism of Zooplankton Aggregation. Science 308, 860–862. https://doi.org/10.1126/science.1107834

Gowan, T.A., Ortega-Ortiz, J.G., Hostetler, J.A., Hamilton, P.K., Knowlton, A.R., Jackson, K.A., George, R.C., Taylor, C.R., Naessig, P.J., 2019. Temporal and demographic variation in partial migration of the North Atlantic right whale. Sci. Rep. 9, 353. https://doi.org/10.1038/s41598-018-36723-3

Grenouillet, G., Buisson, L., Casajus, N., & Lek, S. (2011). Ensemble modelling of species distribution: The effects of geographical and environmental ranges. *Ecography*, *34*(1), 9–17. https://doi.org/10.1111/j.1600-0587.2010.06152.x

Grieve, B.D., Hare, J.A., Saba, V.S., 2017. Projecting the effects of climate change on Calanus finmarchicus distribution within the U.S. Northeast Continental Shelf. Sci. Rep. 7, 6264.

https://doi.org/10.1038/s41598-017-06524-1

Hamilton, P., 2018. A Rare Right Whale Sighting in Iceland [WWW Document]. Cent. Ocean Life. URL https://www.andersoncabotcenterforoceanlife.org/blog/a-rare-right-whale-sighting-in-iceland/ (accessed 9.26.22).

Hays, G.C., 2003. A review of the adaptive significance and ecosystem consequences of zooplankton diel vertical migrations, in: Jones, M.B., Ingólfsson, A., Ólafsson, E., Helgason, G.V., Gunnarsson, K., Svavarsson, J. (Eds.), Migrations and Dispersal of Marine Organisms. Springer Netherlands, Dordrecht, pp. 163–170. https://doi.org/10.1007/978-94-017-2276-6_18

Heath, M.R., Boyle, P.R., Gislason, A., Gurney, W.S.C., Hay, S.J., Head, E.J.H., Holmes, S., Ingvarsdóttir, A., Jónasdóttir, S.H., Lindeque, P., Pollard, R.T., Rasmussen, J., Richards, K., Richardson, K., Smerdon, G., Speirs, D., 2004. Comparative ecology of over-wintering Calanus finmarchicus in the northern North Atlantic, and implications for life-cycle patterns. ICES J. Mar. Sci. 61, 698–708. https://doi.org/10.1016/j.icesjms.2004.03.013

Hirche, H.-J., 1997. Life cycle of the copepod *Calanus hyperboreus* in the Greenland Sea. Mar. Biol. 128, 607–618. https://doi.org/10.1007/s002270050127

Hirche, H.-J., 1996a. The reproductive biology of the marine copepod, Calanus finmarchicus — A review. Ophelia 44, 111–128. https://doi.org/10.1080/00785326.1995.10429842

Hirche, H.-J., 1996b. Diapause in the marine copepod, Calanus finmarchicus — A review. Ophelia 44, 129–143. https://doi.org/10.1080/00785326.1995.10429843

Hirche, H.-J., 1996c. Diapause in the marine copepod, Calanus finmarchicus — A review. Ophelia 44, 129–143. https://doi.org/10.1080/00785326.1995.10429843

Hlista, B., Sosik, H., Martin Traykovski, L., Kenney, R., Moore, M., 2009. Seasonal and interannual correlations between right-whale distribution and calving success and chlorophyll concentrations in the Gulf of Maine, USA. Mar. Ecol. Prog. Ser. 394, 289–302. https://doi.org/10.3354/meps08267

Irigoien, X., 2004. Some ideas about the role of lipids in the life cycle of Calanus finmarchicus. J. Plankton Res. 26, 259–263. https://doi.org/10.1093/plankt/fbh030

IUCN, 2020. Eubalaena glacialis: Cooke, J.G.: The IUCN Red List of Threatened Species 2020: e.T41712A178589687. https://doi.org/10.2305/IUCN.UK.2020-2.RLTS.T41712A178589687.en

Johnson, C.L., Leising, A.W., Runge, J.A., Head, E.J.H., Pepin, P., Plourde, S., Durbin, E.G., 2008. Characteristics of *Calanus finmarchicus* dormancy patterns in the Northwest Atlantic. ICES J. Mar. Sci. 65, 339–350. https://doi.org/10.1093/icesjms/fsm171

Johnson, H., Morrison, D., Taggart, C., 2021. WhaleMap: a tool to collate and display whale survey results in near real-time. J. Open Source Softw. 6, 3094. https://doi.org/10.21105/joss.03094

Kane, J., 2008. A comparison of two zooplankton time series data collected in the Gulf of Maine. J. Plankton Res. 31, 249–259. https://doi.org/10.1093/plankt/fbn119

Kenney, R.D., Hyman, M.A.M., Owen, R.E., Scott, G.P., Winn, H.E., 1986. ESTIMATION OF PREY DENSITIES REQUIRED BY WESTERN NORTH ATLANTIC RIGHT WHALES. Mar. Mammal Sci. 2, 1–13. https://doi.org/10.1111/j.1748-7692.1986.tb00024.x

Kenney, R.D., Mayo, C.A., Winn, H.E., 2020. Migration and foraging strategies at varying spatial scales in western North Atlantic right whales: a review of hypotheses. J Cetacean Res Manage 251–260. https://doi.org/10.47536/jcrm.vi.283

Knowlton, A., Hamilton, P., Marx, M., Pettis, H., Kraus, S., 2012. Monitoring North Atlantic right whale Eubalaena glacialis entanglement rates: a 30 yr retrospective. Mar. Ecol. Prog. Ser. 466, 293–302. https://doi.org/10.3354/meps09923

Knowlton, A.R., Clark, J.S., Hamilton, P.K., Kraus, S.D., Pettis, H.M., Rolland, R.M., Schick, R.S., 2022.

Fishing gear entanglement threatens recovery of critically endangered North Atlantic right whales. Conserv. Sci. Pract. https://doi.org/10.1111/csp2.12736

Krumhansl, K.A., Head, E.J.H., Pepin, P., Plourde, S., Record, N.R., Runge, J.A., Johnson, C.L., 2018. Environmental drivers of vertical distribution in diapausing Calanus copepods in the Northwest Atlantic. Prog. Oceanogr. 162, 202–222. https://doi.org/10.1016/j.pocean.2018.02.018

Laist, D., Knowlton, A., Pendleton, D., 2014. Effectiveness of mandatory vessel speed limits for protecting North Atlantic right whales. Endanger. Species Res. 23, 133–147. https://doi.org/10.3354/esr00586

Lehoux, C., Plourde, S., Lesage, V., 2020. Significance of dominant zooplankton species to the North Atlantic Right Whale potential foraging habitats in the Gulf of St. Lawrence: a bio-energetic approach. DFO Canada.

MacArthur, R. H., & Pianka, E. R. (1966). On optimal use of a patchy environment. *The American Naturalist*, *100*(916), 603–609. https://doi.org/10.1086/282454

Maps, F., Plourde, S., McQuinn, I.H., St-Onge-Drouin, S., Lavoie, D., Chassé, J., Lesage, V., 2015. Linking acoustics and finite-time Lyapunov exponents reveals areas and mechanisms of krill aggregation within the Gulf of St. Lawrence, eastern Canada: Acoustics, FTLE and krill aggregation dynamics. Limnol. Oceanogr. 60, 1965–1975. https://doi.org/10.1002/lno.10145

Maps, F., Plourde, S., Zakardjian, B., 2010. Control of dormancy by lipid metabolism in Calanus finmarchicus: a population model test. Mar. Ecol. Prog. Ser. 403, 165–180. https://doi.org/10.3354/meps08525

Maps, F., Record, N.R., Pershing, A.J., 2014. A metabolic approach to dormancy in pelagic copepods helps explaining inter- and intra-specific variability in life-history strategies. J. Plankton Res. 36, 18–30. https://doi.org/10.1093/plankt/fbt100

Maps, F., Zakardjian, B.A., Plourde, S., Saucier, F.J., 2011. Modeling the interactions between the seasonal and diel migration behaviors of Calanus finmarchicus and the circulation in the Gulf of St. Lawrence (Canada). J. Mar. Syst. 88, 183–202. https://doi.org/10.1016/j.jmarsys.2011.04.004

Mate, B. R., Nieukirk, S. L., & Kraus, S. D. (1997). Satellite-Monitored movements of the northern right whale. *The Journal of Wildlife Management*, *61*(4), 1393–1405. https://doi.org/10.2307/3802143

Mayo, C.A., Letcher, B.H., Scott, S., 2020. Zooplankton filtering efficiency of the baleen of a North Atlantic right whale, Eubalaena glacialis. J Cetacean Res Manage 225–229. https://doi.org/10.47536/jcrm.vi.286

Mayo, C.A., Marx, M.K., 1990. Surface foraging behaviour of the North Atlantic right whale, Eubalaena glacialis, and associated zooplankton characteristics. Can. J. Zool. 68, 2214–2220. https://doi.org/10.1139/z90-308

McLaren, I.A., Head, E., Sameoto, D.D., 2001. Life cycles and seasonal distributions of Calanus finmarchicus on the central Scotian Shelf 58, 12. https://doi-org.acces.bibl.ulaval.ca/10.1139/f01-007

Meyer-Gutbrod, E., Greene, C., Davies, K., Johns, D., 2021. Ocean Regime Shift is Driving Collapse of the North Atlantic Right Whale Population. Oceanography 34, 22–31. https://doi.org/10.5670/oceanog.2021.308

Meyer-Gutbrod, E., Greene, C., Sullivan, P., Pershing, A., 2015. Climate-associated changes in prey availability drive reproductive dynamics of the North Atlantic right whale population. Mar. Ecol. Prog. Ser. 535, 243–258. https://doi.org/10.3354/meps11372

Meyer-Gutbrod, E.L., Greene, C.H., 2018. Uncertain recovery of the North Atlantic right whale in a

changing ocean. Glob. Change Biol. 24, 455–464. https://doi.org/10.1111/gcb.13929

Moore, M., Rowles, T., Fauquier, D., Baker, J., Biedron, I., Durban, J., Hamilton, P., Henry, A., Knowlton, A., McLellan, W., Miller, C., Pace, R., Pettis, H., Raverty, S., Rolland, R., Schick, R., Sharp, S., Smith, C., Thomas, L., van der Hoop, J., Ziccardi, M., 2021. REVIEW Assessing North Atlantic right whale health: threats, and development of tools critical for conservation of the species. Dis. Aquat. Organ. 143, 205–226. https://doi.org/10.3354/dao03578

Murphy, C.T., Marx, M., Martin, W.N., Jiang, H., Lapseritis, J.M., French, A.N., Simmons, N.B., Moore, M.J., 2022. Feeling for food: Can rostro-mental hair arrays sense hydrodynamic cues for foraging North Atlantic right whales? Anat. Rec. 305, 577–591. https://doi.org/10.1002/ar.24858

Neuheimer, A.B., Taggart, C.T., 2007. The growing degree-day and fish size-at-age: the overlooked metric. Can. J. Fish. Aquat. Sci. 64, 375–385. https://doi.org/10.1139/f07-003

Pace, R.M., Corkeron, P.J., Kraus, S.D., 2017. State-space mark-recapture estimates reveal a recent decline in abundance of North Atlantic right whales. Ecol. Evol. 7, 8730–8741. https://doi.org/10.1002/ece3.3406

Pace, R. M., III, Williams, R., Kraus, S. D., Knowlton, A. R., & Pettis, H. M. (2021). Cryptic mortality of North Atlantic right whales. *Conservation Science and Practice*, *3*(2). https://doi.org/10.1111/csp2.346

Pace, R.M., Williams, R., Kraus, S.D., Knowlton, A.R., Pettis, H.M., 2021. Cryptic mortality of North Atlantic right whales. Conserv. Sci. Pract. 3. https://doi.org/10.1111/csp2.346

Pendleton, D., Sullivan, P., Brown, M., Cole, T., Good, C., Mayo, C., Monger, B., Phillips, S., Record, N., & Pershing, A. (2012). Weekly predictions of North Atlantic right whale Eubalaena glacialis habitat reveal influence of prey abundance and seasonality of habitat preferences. *Endangered Species Research*, *18*(2), 147–161. https://doi.org/10.3354/esr00433

Pershing, Jeffrey A. Runge Rebecca J. Jones Nicholas R. Record Andre. "Summer distribution of the planktonic copepod, Calanus finmarchicus, along the coast of the Gulf of Maine." (2012).

Pershing, A. J., & Stamieszkin, K. (2020). The North Atlantic Ecosystem, from Plankton to Whales. *Annual Review of Marine Science*, *12*(1), 339–359. https://doi.org/10.1146/annurev-marine-010419-010752

Pershing, A.J., Pendleton, D., 2021. Can Right Whales Out-Swim Climate Change? Can We? Oceanography 34, 19–21. https://doi.org/10.5670/oceanog.2021.315

Pettis, H. M., Pace, III, R. M., Schick, R. S., & Hamilton, P. K. (2021a). *North Atlantic Right Whale Consortium 2021 annual report card*. North Atlantic Right Whale Consortium. http://dx.doi.org/10.1575/1912/29595

Pettis, H. M., Pace, III, R. M., Schick, R. S., & Hamilton, P. K. (2021b). *North Atlantic Right Whale Consortium 2021 annual report card*. North Atlantic Right Whale Consortium. http://dx.doi.org/10.1575/1912/29595

Pierson, J.J., Batchelder, H., Saumweber, W., Leising, A., Runge, J., 2013. The impact of increasing temperatures on dormancy duration in Calanus finmarchicus. J. Plankton Res. 35, 504–512. https://doi.org/10.1093/plankt/fbt022

Plourde, S., Joly, P., Runge, J., Dodson, J., Zakardjian, B., 2003. Life cycle of Calanus hyperboreus in the lower St. Lawrence Estuary and its relationship to local environmental conditions. Mar. Ecol. Prog. Ser. 255, 219–233. https://doi.org/10.3354/meps255219

Plourde, S., Joly, P., Runge, J.A., Zakardjian, B., Dodson, J.J., 2001. Life cycle of Calanus finmarchicus in the lower St. Lawrence Estuary: the imprint of circulation and late timing of the spring phytoplankton bloom 58, 13. https://doi.org/10.1139/cjfas-58-4-647

Plourde, S., Lehoux, C., Johnson, C.L., Perrin, G., Lesage, V., 2019. North Atlantic right whale (Eubalaena glacialis) and its food: (I) a spatial climatology of Calanus biomass and potential foraging habitats in Canadian waters. J. Plankton Res. 41, 667–685.

https://doi.org/10.1093/plankt/fbz024

Press, A., 2017. North Atlantic right whales could become extinct, US officials say. The Guardian.

Price, W.L., 1977. A controlled random search procedure for global optimisation. The Computer Journal, 20: 367-370

Record, N., Runge, J., Pendleton, D., Balch, W., Davies, K., Pershing, A., Johnson, C., Stamieszkin, K., Ji, R., Feng, Z., Kraus, S., Kenney, R., Hudak, C., Mayo, C., Chen, C., Salisbury, J., Thompson, C., 2019. Rapid Climate-Driven Circulation Changes Threaten Conservation of Endangered North Atlantic Right Whales. Oceanography 32. https://doi.org/10.5670/oceanog.2019.201

Reeves, R.R., Smith, T., Josephson, E.A., 2009. Near-annihilation of a species: Right whaling in the North Atlantic, in: The Urban Whale: North Atlantic Right Whales at the Crossroads. Harvard University Press, Cambridge, Mass., pp. 39–74.

Ross, C. H., Pendleton, D. E., Tupper, B., Brickman, D., Zani, M. A., Mayo, C. A., & Record, N. R. (2021). Projecting regions of North Atlantic right whale, Eubalaena glacialis, habitat suitability in the Gulf of Maine for the year 2050. *Elementa: Science of the Anthropocene*, *9*(1). https://doi.org/10.1525/elementa.2020.20.00058

Runge, J., Simard, Y., 1990. Zooplankton of the St. Lawrence Estuary: The Imprint of Physical Processes on its Composition and Distribution, in: Oceanography of a Large-Scale Estuarine System. Springer New York, New York, NY, pp. 296–320. https://doi.org/10.1007/978-1-4615-7534-4

Saba, V.S., Griffies, S.M., Anderson, W.G., Winton, M., Alexander, M.A., Delworth, T.L., Hare, J.A., Harrison, M.J., Rosati, A., Vecchi, G.A., Zhang, R., 2016. Enhanced warming of the Northwest Atlantic Ocean under climate change. J. Geophys. Res. Oceans 121, 118–132. https://doi.org/10.1002/2015JC011346

Sameoto, D., Herman, A., 1990. Life cycle and distribution of Calanus finmarchicus in deep basins on the Nova Scotia shelf and seasonal changes in Calanus spp. Mar. Ecol. Prog. Ser. 66, 225–237. https://doi.org/10.3354/meps066225

Saumweber, W.J., Durbin, E.G., 2006. Estimating potential diapause duration in Calanus finmarchicus. Deep Sea Res. Part II Top. Stud. Oceanogr. 53, 2597–2617. https://doi.org/10.1016/j.dsr2.2006.08.003

Schmid, M.S., Fortier, L., 2019. The intriguing co-distribution of the copepods Calanus hyperboreus and Calanus glacialis in the subsurface chlorophyll maximum of Arctic seas. Elem. Sci. Anthr. 7, 50. https://doi.org/10.1525/elementa.388

Segurado, P., & Araújo, M. B. (2004). An evaluation of methods for modelling species distributions. *Journal of Biogeography*, *31*(10), 1555–1568. https://doi.org/10.1111/j.1365-2699.2004.01076.x

Seidov, D., Mishonov, A., Parsons, R., 2021. Recent warming and decadal variability of Gulf of Maine and Slope Water. Limnol. Oceanogr. 66, 3472–3488. https://doi.org/10.1002/lno.11892

Simard, Y., Lacroix, G., Legendre, L., 1985. In situ twilight grazing rhythm during diel vertical migrations of a scattering layer of Calanus finmarchicus 1: In situ grazing rhythms. Limnol. Oceanogr. 30, 598–606. https://doi.org/10.4319/lo.1985.30.3.0598

Smith, G.C., Liu, Y., Benkiran, M., Chikhar, K., Surcel Colan, D., Gauthier, A.-A., Testut, C.-E., Dupont, F., Lei, J., Roy, F., Lemieux, J.-F., Davidson, F., 2021. The Regional Ice Ocean Prediction System v2: a pan-Canadian ocean analysis system using an online tidal harmonic analysis. Geosci. Model Dev. 14, 1445–1467. https://doi.org/10.5194/gmd-14-1445-2021

Soetaert, K. and P.M.J. Herman, 2009. A Practical Guide to Ecological Modelling. Using R as a Simulation Platform. Springer, 372 pp.

Sorochan, K.A., Plourde, S., Baumgartner, M.F., Johnson, C.L., 2021(A). Availability, supply, and aggregation of prey (Calanus spp.) in foraging areas of the North Atlantic right whale

(Eubalaena glacialis). ICES Journal of Marine Science 78, 3498–3520. https://doi.org/10.1093/icesjms/fsab200

Sorochan, K.A., Brennan, C.E., Plourde, S., Johnson, C.L., 2021(B). Spatial variation and transport of abundant copepod taxa in the southern Gulf of St. Lawrence in autumn. J. Plankton Res. 43, 908–926. https://doi.org/10.1093/plankt/fbab066

Sorochan, K.A., Plourde, S., Morse, R., Pepin, P., Runge, J., Thompson, C., Johnson, C.L., 2019. North Atlantic right whale (Eubalaena glacialis) and its food: (II) interannual variations in biomass of Calanus spp. on western North Atlantic shelves. J. Plankton Res. 41, 687–708. https://doi.org/10.1093/plankt/fbz044

Thewissen, J.G.M., George, J., Rosa, C., Kishida, T., 2011. Olfaction and brain size in the bowhead whale (Balaena mysticetus). Mar. Mammal Sci. 27, 282–294. https://doi.org/10.1111/j.1748-7692.2010.00406.x

Vanderlaan, A., Taggart, C., Serdynska, A., Kenney, R., Brown, M., 2008. Reducing the risk of lethal encounters: vessels and right whales in the Bay of Fundy and on the Scotian Shelf. Endanger. Species Res. 4, 283–297. https://doi.org/10.3354/esr00083

Visser, A.W., Grønning, J., Jónasdóttir, S.H., 2017. Calanus hyperboreus and the lipid pump: Calanus hyperboreus and the lipid pump. Limnol. Oceanogr. 62, 1155–1165. https://doi.org/10.1002/lno.10492

Vogedes, D.L., 2014. Calanus spp. in the Arctic ecosystem - a story on predation, distribution and methodology.

Woodson, C.B., McManus, M.A., 2007. Foraging behavior can influence dispersal of marine organisms. Limnol. Oceanogr. 52, 2701–2709. https://doi.org/10.4319/lo.2007.52.6.2701

Zakardjian, B.A., Runge, J.A., Plourde, S., Gratton, Y., 1999. A biophysical model of the interaction between vertical migration of crustacean zooplankton and circulation in the Lower St. Lawrence Estuary. Can. J. Fish. Aquat. Sci. 56, 2420–2432. https://doi.org/10.1139/f99-095

Zakardjian, B.A., 2003. Effects of temperature and circulation on the population dynamics of Calanus finmarchicus in the Gulf of St. Lawrence and Scotian Shelf: Study with a coupled, three-dimensional hydrodynamic, stage-based life history model. J. Geophys. Res. 108, 8016. https://doi.org/10.1029/2002JC001410